EUROPEAN ORGANIZATION FOR NUCLEAR RESEARCH (CERN)
FERMILAB-PUB-11-741-CMS

CERN-PH-EP/2011-049
2011/09/30

CMS-QCD-10-008

Charged particle transverse momentum spectra in pp collisions at $\sqrt{s}$ = 0.9 and 7 TeV

The CMS Collaboration*

arXiv:1104.3547v2 [hep-ex] 29 Sep 2011

Abstract

The charged particle transverse momentum (p_{T}) spectra are presented for pp collisions at $\sqrt{s} = 0.9$ and 7 TeV. The data samples were collected with the CMS detector at the LHC and correspond to integrated luminosities of 231 $\mu\mathrm{b}^{-1}$ and 2.96 pb^{-1}, respectively. Calorimeter-based high-transverse-energy triggers are employed to enhance the statistical reach of the high-p_{T} measurements. The results are compared with leading and next-to-leading order QCD and with an empirical scaling of measurements at different collision energies using the scaling variable $x_{\mathrm{T}} \equiv 2p_{\mathrm{T}}/\sqrt{s}$ over the p_{T} range up to 200 GeV/c. Using a combination of x_{T} scaling and direct interpolation at fixed p_{T}, a reference transverse momentum spectrum at $\sqrt{s} = 2.76$ TeV is constructed, which can be used for studying high-p_{T} particle suppression in the dense QCD medium produced in heavy-ion collisions at that centre-of-mass energy.

Submitted to the Journal of High Energy Physics

*See Appendix A for the list of collaboration members

Operated by Fermi Research Alliance, LLC under Contract No. De-AC02-07CH11359 with the United States Department of Energy.

1 Introduction

The charged particle transverse momentum (p_T) spectrum is an important observable for understanding the fundamental quantum chromodynamic (QCD) interactions involved in proton-proton collisions. While the energy dependence of the bulk of particle production with p_T below a few GeV/c is typically described either empirically or with phenomenological models, the rest of the spectrum can be well described by a convolution of parton distribution functions, the hard-scattering cross section from perturbative calculations, and fragmentation functions. Such a prescription has been generally successful over a large range of lower energy pp and p$\bar{\text{p}}$ collisions [1–7]. Along with measurements of the jet production cross section and fragmentation functions, measurements of high-p_T spectra provide a test of factorised perturbative QCD (pQCD) [8] at the highest collision energy to date.

In addition to its relevance to the understanding of pQCD, the charged particle spectrum in pp collisions will be an important reference for measurements of high-p_T particle suppression in the dense QCD medium produced in heavy-ion collisions. At the Relativistic Heavy Ion Collider (RHIC), the sizable suppression of high-p_T particle production, compared to the spectrum expected from a superposition of a corresponding number of pp collisions, was one of the first indications of strong final-state medium effects [9–12]. A similar measurement of nuclear modification to charged particle p_T spectra has been one of the first heavy-ion results at the Large Hadron Collider (LHC) [13]. The reference spectrum for the PbPb collisions at $\sqrt{s_{NN}} = 2.76$ TeV per nucleon can be constrained by interpolating between the pp spectra measured at $\sqrt{s}$ = 0.9 and 7 TeV.

In this paper, the phase-space-invariant differential yield $E\,d^3N_{ch}/dp^3$ is presented for primary charged particles with energy (E) and momentum (p), averaged over the pseudorapidity acceptance of the Compact Muon Solenoid (CMS) tracking system ($|\eta| < 2.4$). The pseudorapidity is defined as –ln[tan(θ/2)], with θ being the polar angle of the charged particle with respect to the counterclockwise beam direction. The number of primary charged particles (N_{ch}) is defined to include decay products of particles with proper lifetimes less than 1 cm. Using the integrated luminosities calculated in Refs. [14, 15] with an estimated uncertainty of 11% and 4% at $\sqrt{s} = 0.9$ and 7 TeV, respectively, the differential cross sections are constructed and compared to a scaling with the variable $x_T \equiv 2p_T/\sqrt{s}$. Such a scaling has already been observed for p$\bar{\text{p}}$ measurements at lower collision energies [4, 5, 16, 17]. For consistency with the CDF measurements at $\sqrt{s} = 0.63$, 1.8, and 1.96 TeV, the pseudorapidity range of the x_T distributions has been restricted to $|\eta| < 1.0$.

Finally, using the new measurements presented in this paper, as well as previously measured pp and p$\bar{\text{p}}$ cross sections, an estimate of the differential transverse momentum cross section is constructed at the interpolated energy of $\sqrt{s} = 2.76$ TeV, corresponding to the nucleon-nucleon centre-of-mass energy of PbPb collisions recorded at the LHC.

The paper is organised as follows: Section 2 contains a description of the CMS detector; Section 3 describes the trigger and event selection; Sections 4 and 5 detail the reconstruction and selection of primary vertices and tracks; Section 6 explains the characterisation of events based on the leading-jet transverse energy; Section 7 describes the various applied corrections and systematic uncertainties; Section 8 presents the final invariant differential yields and comparisons to data and simulation; and Section 9 discusses the interpolation procedures used to construct a reference spectrum at $\sqrt{s} = 2.76$ TeV.

2 The CMS Detector

A detailed description of the CMS experiment can be found in Ref. [18]. The central feature of the CMS apparatus is a superconducting solenoid of 6 m internal diameter, providing an axial magnetic field of 3.8 T. Immersed in the magnetic field are the pixel tracker, the silicon strip tracker, the lead tungstate crystal electromagnetic calorimeter (ECAL), and the brass/scintillator hadron calorimeter (HCAL). Muons are measured in gas ionisation detectors embedded in the steel return yoke.

The CMS experiment uses a right-handed coordinate system, with the origin at the nominal interaction point, the x axis pointing to the centre of the LHC ring, the y axis pointing up perpendicular to the plane of the LHC, and the z axis along the counterclockwise beam direction. The azimuthal angle, ϕ, is measured in the (x, y) plane.

The tracker consists of 1440 silicon pixel and 15 148 silicon strip detector modules and measures charged particle trajectories within the nominal pseudorapidity range $|\eta| < 2.4$. The pixel tracker consists of three 53.3 cm-long barrel layers and two endcap disks on each side of the barrel section. The innermost barrel layer has a radius of 4.4 cm, while for the second and third layers the radii are 7.3 cm and 10.2 cm, respectively. The tracker is designed to provide an impact parameter resolution of about 100 μm and a transverse momentum resolution of about 0.7 % for 1 GeV/c charged particles at normal incidence ($\eta = 0$) [19].

The tracker was aligned as described in Ref. [20] using cosmic ray data prior to the LHC commissioning. The precision achieved for the positions of the detector modules with respect to particle trajectories is 3–4 μm in the barrel for the coordinate in the bending plane (ϕ).

Two elements of the CMS detector monitoring system, the beam scintillator counters (BSC) [18, 21] and the beam pick-up timing for the experiments devices (BPTX) [18, 22], were used to trigger the detector readout. The BSCs are located at a distance of 10.86 m from the nominal interaction point (IP), one on each side, and are sensitive in the $|\eta|$ range from 3.23 to 4.65. Each BSC is a set of 16 scintillator tiles. The BSC elements have a time resolution of 3 ns, an average minimum ionising particle detection efficiency of 95.7%, and are designed to provide hit and coincidence rates. The two BPTX devices, located around the beam pipe at a position of $z = \pm 175$ m from the IP, are designed to provide precise information on the bunch structure and timing of the incoming beam, with better than 0.2 ns time resolution.

The two steel/quartz-fibre forward calorimeters (HF), which extend the calorimetric coverage beyond the barrel and endcap detectors to the $|\eta|$ region between 2.9 and 5.2, were used for further offline selection of collision events.

The detailed Monte Carlo (MC) simulation of the CMS detector response is based on GEANT4 [23]. Simulated events were processed and reconstructed in the same manner as collision data.

3 Event Selection

This analysis uses data samples collected from 0.9 and 7 TeV pp collisions in the first months of the 2010 LHC running, corresponding to integrated luminosities of $(231 \pm 25)\,\mu\text{b}^{-1}$ and $(2.96 \pm 0.12)\,\text{pb}^{-1}$, respectively [14, 15]. This section gives a brief description of the requirements imposed to select good events for this analysis. A more detailed description of the CMS trigger selections can be found in Ref. [24].

First, a minimum bias trigger was used to select events with a signal in any of the BSC tiles, coincident with a signal from either of the two BPTX detectors, indicating the presence of at

least one proton bunch crossing the interaction point. From this sample, collision events were selected offline by requiring a coincidence of BPTX signals, indicating the presence of both beams.

To select preferentially non-single-diffractive (NSD) events, at least one forward calorimeter (HF) tower with energy deposition $E > 3\,\text{GeV}$ in each of the forward and backward hemispheres was required. Events with beam-halo muons crossing the detector were identified and rejected based on the time difference between BSC hits on either side of the interaction point. Beam-induced background events, producing anomalous numbers of low-quality tracks, were rejected by requiring that at least 25% of the charged particles reconstructed in the pixel–silicon tracking system satisfied the *highPurity* criterion. This criterion, described in Ref. [25], consists of numerous selections on the properties of the tracks, including the normalised χ^2, the compatibility with the beamline and primary vertices, the number of hit layers, the number of '3D' layers, and the number of lost layers. The selection on the fraction of *highPurity* tracks was only applied to events with more than 10 tracks, providing a clean separation between real pp collisions and beam backgrounds. The remaining non-collision event fraction, determined by applying the same selections to events where only a single beam was crossing the interaction point, is estimated to be less than 2×10^{-5}. Events were required to have at least one primary vertex, reconstructed according to the description in the following section from triplets of pixel hits. A further requirement, namely at least one vertex found from fully reconstructed tracks (see next section for details) with number of degrees of freedom ($Ndof$) greater than four, was imposed to improve the robustness against triggered events containing multiple pp collisions, i.e., "event pileup". The loss in event selection efficiency from the fully-reconstructed-track vertex compared to the pixel vertex alone was determined entirely from data, based on a subset of early runs with negligible event pileup. The percentage of events remaining after each selection step is presented in Table 1.

For a large part of the 7 TeV data collection, the minimum bias trigger paths had to be prescaled by large factors because of the increasing instantaneous luminosity of the LHC. In order to maximise the p_{T} reach of the charged particle transverse momentum measurement at this centre-of-mass energy, two high-level trigger (HLT) paths were used that selected events with minimum uncorrected transverse jet energies (E_{T}) of 15 and 50 GeV, based only on information from the calorimeters. While the higher threshold path was not prescaled during the 7 TeV data-taking period corresponding to the $2.96\,\text{pb}^{-1}$ used in this analysis, the lower threshold path had to be prescaled for a significant fraction of this sample. The 0.9 TeV data sample consists of 6.8 million minimum bias triggered events, while the 7 TeV sample is composed of 18.7 million minimum bias events, and 1.4 (5.6) million events selected with the HLT minimum-E_{T} values of 15 (50) GeV.

The selection efficiency for NSD events was determined based on simulated events from the PYTHIA [26] event generator (version 6.420, tune D6T [27]) that were subsequently passed through a Monte Carlo simulation of the CMS detector response. The resulting event selection efficiency as a function of the multiplicity of reconstructed charged particles is shown for 7 TeV collisions in Fig. 1a. The corresponding event selection efficiency is calculated by the same technique for the 0.9 TeV data (not shown). Based on events simulated with PHOJET [28, 29] and PYTHIA, the remaining fraction of single-diffractive (SD) events in the selected sample was estimated to be $(5 \pm 1)\%$ and $(6 \pm 1)\%$ for the 0.9 and 7 TeV data, respectively.

Table 1: Summary of event selection steps applied to the 0.9 and 7 TeV collision data sets and the percentage of events from the original minimum bias samples that remain after each step.

Collision energy	0.9 TeV	7 TeV
Selection	Percentage passing each selection cut	
One BSC + one BPTX	100.0	100.0
BPTX coincidence	94.49	90.05
Beam halo rejection	94.08	89.83
HF coincidence	73.27	83.32
Beam background rejection	73.26	83.32
Valid pixel-track vertex	70.14	82.48
Quality full-track vertex	64.04	77.35

4 Primary Vertex

In this analysis, two separate algorithms are employed to determine the primary vertex position. The first is a highly efficient algorithm based on pixel triplet tracks that requires a minimum of just a single track consistent with the beam-spot position. The position of the beam-spot, taken as the centre of the region where the LHC beams collide, is calculated for each LHC fill based on the average over many events of the three-dimensional fitted vertex positions [25]. The second vertex-finding algorithm, based on fully reconstructed tracks with hits also in the silicon strip tracker, is less efficient in selecting low-multiplicity events, but more robust in discriminating against event pileup. Since pileup is significant over the majority of the analysed data sample, only the fully-reconstructed-track vertex is used to construct the raw charged particle momentum spectra. The raw spectra are subsequently corrected for the fraction of events with fewer than four tracks (and the fraction of tracks in such low-multiplicity events), based on a subset of the event sample selected with the more efficient pixel-track vertex requirement during collision runs with negligible event pileup.

To determine the z position of the pixel vertex in each event, tracks consisting of three pixel hits are constructed with a minimum p_{T} of 75 MeV/c from a region within a transverse distance of 0.2 cm from the beam axis. The x and y positions of the pixel vertex are taken from the transverse position of the beam axis. Fitted tracks are selected based on the requirement that the transverse impact parameter is less than three times the quadratic sum of the transverse errors on the track impact parameter and the beam axis position. The selected tracks are then passed to an agglomerative algorithm [30], which iteratively clusters the tracks into vertex-candidates. The procedure is halted when the distance between nearest clusters, normalised by their respective position uncertainties, reaches 12. Only vertices consisting of at least two tracks are kept, except when the event contains a single reconstructed track, which occurs in 1.67% (0.99%) of the events at $\sqrt{s} = 0.9$ (7) TeV. In the case of multiple vertex-candidates, only the vertex with the most associated tracks is kept. While this occurs in as many as 20% of events, the rejected vertex typically has very few associated tracks and is highly correlated in z position to the vertex with the most associated tracks. These characteristics imply that the rejected vertices are not from event pileup, but rather from tracks in the tails of the impact parameter distribution that are not agglomerated into the primary vertex.

The fully-reconstructed-track vertex algorithm begins from a set of tracks selected according to their transverse impact parameter to the beam-spot (< 2 cm), number of hits (> 6), and normalised χ^2 (< 20). These tracks are passed to an adaptive vertex fitter, in which tracks are as-

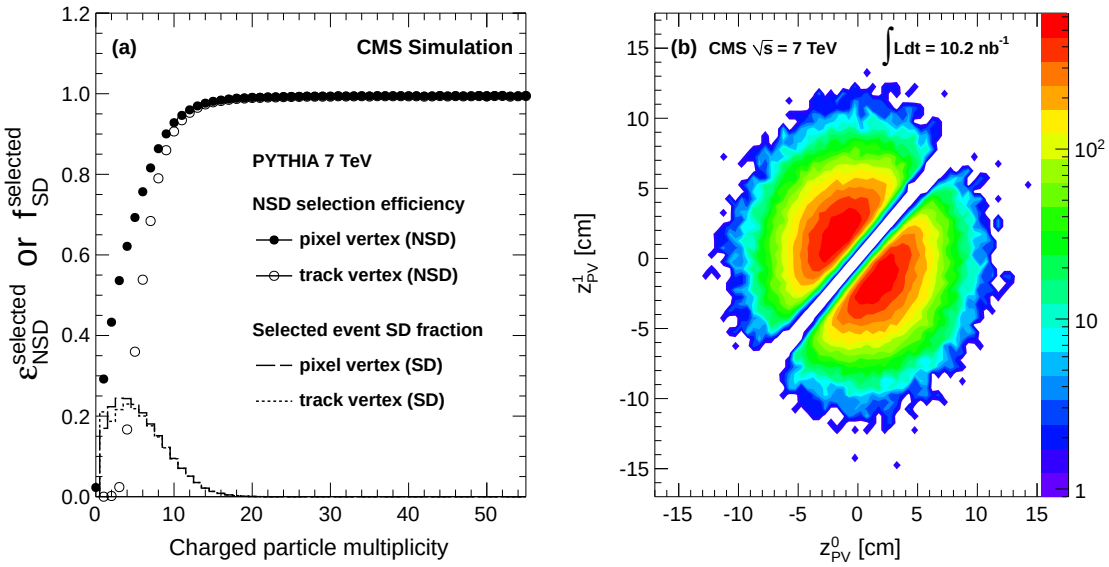

Figure 1: (a) The efficiency ($\varepsilon_{\mathrm{NSD}}^{\mathrm{selected}}$ in Eq. (2)) for selecting non-single-diffractive (NSD) events as a function of the multiplicity of reconstructed charged particles in the tracker acceptance ($|\eta| < 2.4$) after applying the full event selection described in the text, including a single pixel-track vertex (filled circles) and additionally requiring a fully-reconstructed-track vertex with $Ndof > 4$ (open circles) as described in Section 4. Also, the remaining single-diffractive (SD) fraction ($f_{\mathrm{SD}}^{\mathrm{selected}}$ in Eq. (2)) as a function of charged particle multiplicity for the same selections (solid and dashed lines). (b) Correlation between the z positions, z_{PV}^{0} and z_{PV}^{1}, of the two vertices with the most associated tracks for measured events with more than one fully-reconstructed-track vertex satisfying the quality selections.

signed a weight between 0 and 1 according to their compatibility with the common vertex [25]. Quality vertices are further required to have more than four degrees of freedom ($Ndof$), corresponding to at least four tracks with weights of approximately one. For events with multiple reconstructed vertices passing the quality selection, the correlation between the z positions of the two vertices with the most associated tracks is shown in Fig. 1b. Other than the diagonal region without multiple vertices, expected from the algorithmic parameter of at least a 1 cm separation, the uncorrelated positions of the two vertices are indicative of random event pileup.

The event pileup rate is estimated from the fraction of events with multiple reconstructed vertices, after correcting for vertices that are not found because of their proximity. The beam conditions varied over the analysed minimum bias data samples, such that the corrected fraction of pileup events is in the range (0.4–7.5)%. The uncertainty on the event pileup fraction, determined from the largest correction to the multiple-vertex fraction, is a constant factor of 0.2% and 1.2% for the 0.9 and 7 TeV data, respectively.

5 Track Selection

This analysis uses tracks from the standard CMS reconstruction algorithm, which consists of multiple iterations of a combinatorial track finder based on various seeding layer patterns [31]. After each iteration, hits belonging unambiguously to tracks in the previous step are removed from consideration for subsequent steps.

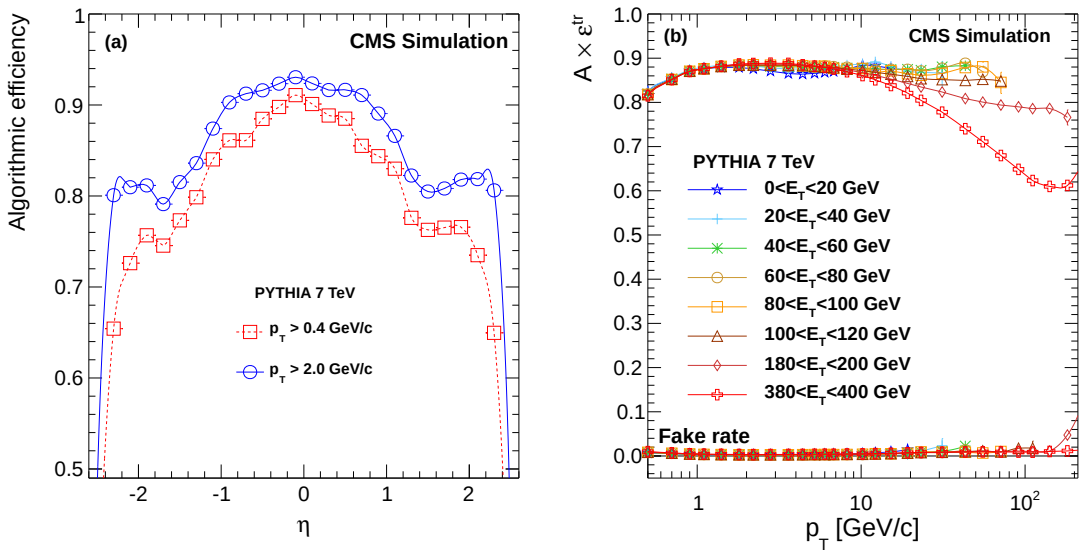

Figure 2: (a) The algorithmic tracking efficiency for two different momentum ranges as a function of η. (b) The product of geometrical acceptance (A) with tracking efficiency ($\varepsilon^{\mathrm{tr}}$) (upper points) and the misidentification ('fake') rate (lower points) as a function of transverse momentum for tracks with $|\eta| < 1$ in bins of corrected leading-jet transverse energy.

In order to minimise the contribution from misidentified tracks and tracks with poor momentum resolution, a number of quality selections are applied. These include the *highPurity* selection mentioned in Section 3, the requirement of at least five hits on the track, the normalized χ^2 per degree of freedom divided by the number of tracker layers used in the fit less than a maximum value which varies from 0.48 and 0.07 depending on η and p_{T}, and a relative momentum uncertainty of less than 20%. Furthermore, to reject non-primary tracks (i.e., the products of weak decays and secondary interactions with detector material), only the pixel-seeded tracking iterations are used, and selections are placed on the impact parameter of the tracks with respect to the primary vertex position. Specifically, the transverse and longitudinal impact parameters are required to be less than 0.2 cm and also less than 3 times the sum in quadrature of the uncertainties on the impact parameter and the corresponding vertex position. In the case of multiple quality reconstructed vertices in the minimum bias event samples, tracks that pass the impact parameter selections with respect to any vertex are used in the analysis. The number of events, by which the track p_{T} distribution is normalised, is then scaled by a factor to account for the event pileup fraction. In contrast, for the jet-triggered samples, tracks are selected based on the impact parameter with respect to the single vertex responsible for the trigger. The primary vertex of the hard-scattering process is identified as the vertex with the largest value of $\sum p_{\mathrm{T}}^2$ for the associated fitted tracks.

With the above-mentioned selections applied to the reconstructed tracks, the algorithmic efficiency determined from simulated PYTHIA events is greater than 85% (80%) for tracks with transverse momentum above 2.0 (0.4) GeV/c averaged over $|\eta| < 2.4$ (Fig. 2a). In the same kinematic region, misidentified and non-primary tracks are each below 1%, while multiple reconstruction occurs for less than 0.01% of tracks.

6 Event Classification by Leading-Jet Energy

All events in this analysis are classified according to the transverse energy of the most energetic reconstructed jet, defined as the leading jet. Jets are reconstructed from calorimeter deposits alone using the anti-k_T algorithm [32] with cone radius $R = \sqrt{(\Delta\phi)^2 + (\Delta\eta)^2} = 0.5$. The measured energy of the jet is adjusted according to corrections based on a MC description of the CMS calorimeter response with a 3–6% uncertainty on the jet energy scale [33].

The motivation for classifying events according to the leading-jet transverse energy is twofold. First, the degrading effect of the local-track density on the high-p_T tracking performance (e.g., inside a jet) can be parametrised according to this variable. Based on events simulated with PYTHIA in minimum bias and QCD samples with various thresholds on the hard-scattering scale ($\hat{p}_T$), the efficiency and misidentification rates of the selected tracks are estimated as a function of transverse momentum in bins of leading-jet transverse energy (see Fig. 2b). Second, as discussed in Section 3, calorimeter-based triggers with leading-jet transverse energy thresholds of 15 GeV (Jet15U) and 50 GeV (Jet50U) were used to extend the p_T reach of the 7 TeV measurement.

To avoid potential biases from the jet-trigger selection, it is desirable to operate in a region where the trigger is fully efficient. The region above which the jet trigger with an uncorrected energy threshold of 15 GeV becomes fully efficient is determined by first plotting the leading-jet E_T distribution for a sample of events selected with the prescaled minimum bias trigger and the offline selections described in Section 3. This distribution is then compared to the subset of those events which also fire the 15 GeV jet trigger as a function of corrected transverse energy. The resulting ratio is the trigger efficiency curve presented in the lower panel of Fig. 3a. The 15 GeV jet trigger achieves more than 99% efficiency at a corrected energy of $E_T = 45$ GeV. The analogous procedure is repeated on a sample of events selected by the 15 GeV jet trigger to determine that the 50 GeV jet trigger becomes fully efficient above $E_T = 95$ GeV. For the trigger efficiency study, an early subset of the data (10.2 nb^{-1}) was used, because the minimum bias and lower-threshold jet triggers were highly prescaled in the later runs. In the upper panel of Fig. 3a, the E_T distributions from the jet-triggered sample are normalised per equivalent minimum bias event by matching their integrals in the regions where the triggers are fully efficient.

For the 7 TeV analysis, events are divided into three classes based on leading-jet E_T: below 60 GeV, between 60 and 120 GeV, and above 120 GeV. Since each event is uniquely assigned to one such leading-jet E_T range, the overall dN_{ch}/dp_T distribution is simply the sum of the spectra from the three ranges, each corresponding to a fully-efficient HLT selection (i.e., minimum bias, 15 GeV jet trigger, and 50 GeV jet trigger). The contributions to the spectra from the jet-triggered events are normalised per selected minimum bias event; the fraction of minimum bias events containing a leading jet with greater than either 60 or 120 GeV is calculated as shown in Fig. 3a by matching the fully-efficient regions of the leading-jet E_T distributions. The three contributions to the combined charged particle transverse momentum spectrum are shown in Fig. 3b. The lower panel of that figure compares the combined spectrum first to the minimum bias spectrum alone and then to a spectrum constructed with the addition of only the lower-threshold jet trigger. These are all in good agreement within their respective statistical uncertainties. A p_T-dependent systematic uncertainty of 0–4% is attributed to the normalisation of the contributions from the triggered samples. This value is determined by changing the leading-jet E_T ranges that separate the three samples (e.g., to $E_T = 40$ and 100 GeV), by basing the normalisation directly on the HLT prescale values, and by comparing the normalisations determined from different subsets of the full data sample.

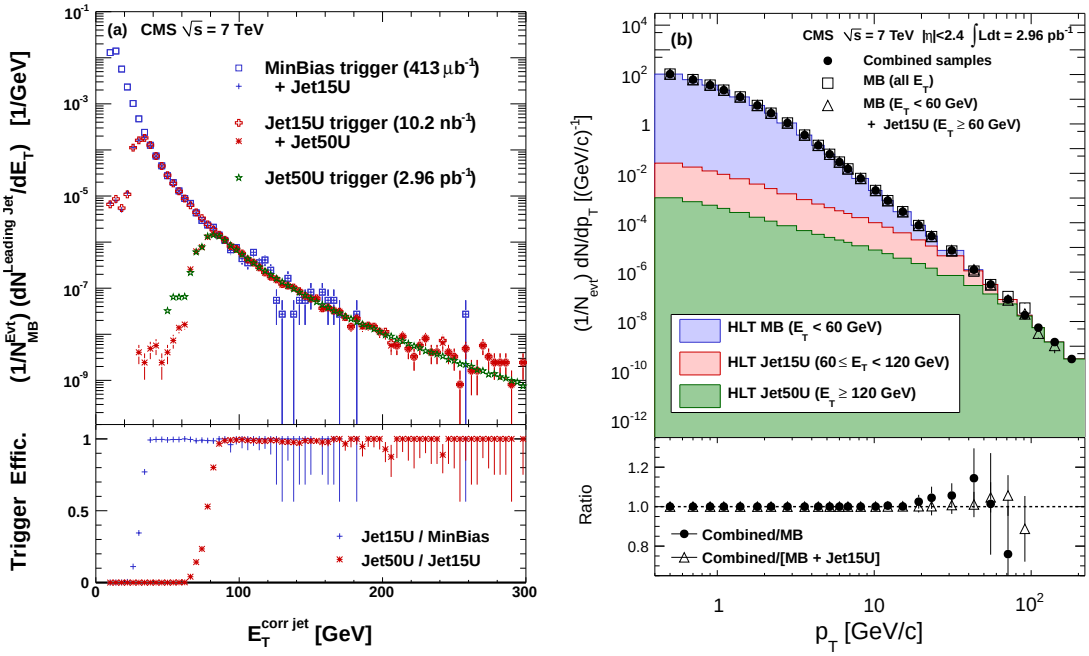

Figure 3: (a) Upper panel: distributions of the corrected transverse energy of leading jets normalised by the number of selected minimum bias events $N_{\mathrm{MB}}^{\mathrm{Evt}}$. Lower panel: the efficiency turn-on curves for the jet triggers with uncorrected energy thresholds of 15 and 50 GeV. (b) Upper panel: the three contributions to the charged particle transverse momentum spectrum and their sum (solid circles). Open squares show the minimum bias spectrum for all values of leading-jet E_{T}; open triangles show the spectrum with the addition of only the lower threshold jet trigger. Lower panel: the ratio of the combined spectrum to minimum bias only (solid circles) and with the addition of only the lower threshold jet trigger (open triangles).

7 Corrections and Systematic Uncertainties

To obtain the final phase-space-invariant charged particle differential momentum distribution, a number of corrections must be applied to the raw distributions of reconstructed charged particles, according to the following equation:

$$E\frac{d^3N_{\mathrm{ch}}}{dp^3}(p_{\mathrm{T}},\eta) = \frac{\sum_{M,E_{\mathrm{T}}^{\mathrm{jet}}} N_{\mathrm{track}}^{\mathrm{raw}}(M,E_{\mathrm{T}}^{\mathrm{jet}},p_{\mathrm{T}},\eta)\cdot w_{\mathrm{tr}}(p_{\mathrm{T}},\eta,E_{\mathrm{T}}^{\mathrm{jet}})\cdot w_{\mathrm{ev}}(M)}{2\pi p_{\mathrm{T}}\cdot\Delta p_{\mathrm{T}}\cdot\Delta\eta\cdot\sum_M N^{\mathrm{selected}}(M)\cdot(1-f_{\mathrm{NSD}}^{0})^{-1}\cdot(1+f^{\mathrm{pileup}})\cdot w_{\mathrm{ev}}(M)}, \quad (1)$$

where $N_{\mathrm{track}}^{\mathrm{raw}}$ is the raw number of tracks in a bin with transverse momentum width Δp_{T} and pseudorapidity width $\Delta\eta$, and N^{selected} is the number of selected events. An event weight w_{ev} (see Eq. (2)) is applied as a function of the multiplicity of reconstructed charged particles (M), while a track weight w_{tr} (see Eq. (3)) is applied for each M and leading-jet transverse energy ($E_{\mathrm{T}}^{\mathrm{jet}}$), as a function of p_{T}; the final results are summed over M and $E_{\mathrm{T}}^{\mathrm{jet}}$. The number of selected events is corrected for the fraction of NSD events (f_{NSD}^{0}) that have zero reconstructed tracks in the tracker acceptance of $|\eta| < 2.4$ (about 5%) and for the pileup event fraction (f^{pileup}).

The multiplicity-dependent event weight w_{ev} accounts for the efficiency of the event selection for accepting NSD events ($\varepsilon_{\mathrm{NSD}}^{\mathrm{selected}}$) and for the fraction of SD events ($f_{\mathrm{SD}}^{\mathrm{selected}}$) that contaminate

Table 2: Summary of the various contributions to the estimated systematic uncertainty.

Source	Uncertainty [%]	
Collision energy	0.9 TeV	7 TeV
Event selection	3.2	3.5
Pileup effect on vertexing	0.2	1.2
Acceptance	1.5	1.5
Reconstruction efficiency	2.2	2.2
Occupancy effect on efficiency	0.0–0.5	0.0–2.8
Misidentified track rate	0.3–1.0	0.3–3.0
Correction for secondary particles	1.0	1.0
Momentum resolution and binning	0.3–1.5	0.3–2.7
Normalisation of jet-triggered spectra	–	0.0–4.0
Total	4.3–4.7	4.7–7.9
Total excluding event selection uncertainty	2.9–3.4	3.1–7.1
Total including luminosity uncertainty	11.4–11.6	5.1–8.1

the selected sample (about 5% overall):

$$w_{\mathrm{ev}}(M) = \frac{1}{\varepsilon_{\mathrm{NSD}}^{\mathrm{selected}}}(1 - f_{\mathrm{SD}}^{\mathrm{selected}}). \tag{2}$$

The correction factor w_{tr}, by which each track is weighted, is calculated for each bin in transverse momentum, pseudorapidity, and leading-jet transverse energy. This factor accounts for the geometric detector acceptance (A) and algorithmic tracking efficiency ($\varepsilon^{\mathrm{tr}}$), as well as the fraction of tracks corresponding to the same, multiply reconstructed charged particle (D), the fraction of tracks corresponding to a non-primary charged particle (S), and the fraction of misidentified ('fake') tracks that do not correspond to any charged particle (F):

$$w_{\mathrm{tr}}(p_{\mathrm{T}}, \eta, E_{\mathrm{T}}^{\mathrm{jet}}) = \frac{(1-F)\cdot(1-S)}{A \cdot \varepsilon^{\mathrm{tr}} \cdot (1+D)}. \tag{3}$$

The common uncertainty related to the triggering and event selection efficiency is discussed in detail in Ref. [34]. Contributions from uncertain diffractive-event fractions and detector inefficiencies in the BSC and HF combine to contribute a scale error of $\pm 3.5\%$ to the total systematic uncertainty at $\sqrt{s} = 7$ TeV (see Table 2). At $\sqrt{s} = 0.9$ TeV, the diffractive fractions are slightly better constrained, hence an uncertainty of $\pm 3.2\%$ is assigned.

Using simulated events generated with PYTHIA tune D6T, the various terms in Eq. (3) are estimated by matching selected reconstructed tracks to simulated tracks based on the requirement that they share 75% of their hits. As an example, the algorithmic efficiency ($\varepsilon^{\mathrm{tr}}$) versus η is presented in Fig. 2a. The slight asymmetry between the positive and negative hemispheres is attributed to a slightly displaced beam-spot and the distribution of dead channels in the tracker. The systematic uncertainties assigned to the various tracking corrections are discussed below and are summarised, along with the total systematic uncertainty, in Table 2.

The uncertainty on the geometrical acceptance of the tracker was estimated from three sources. First, the efficiency of the pixel hit reconstruction was estimated from a data-driven technique

involving the projection of two-hit combinations (called tracklets) onto the third layer in search of a compatible hit. The observed efficiency of $(99.0 \pm 0.5)\%$ leads to a 0.3% uncertainty on the acceptance of pixel-seeded tracks. Second, the variation of the geometrical acceptance was estimated for a variety of generator tunes including PYTHIA8 [35] and the Perugia0 [36] tune of PYTHIA. Third, the variation was estimated after shifting the generated beam-spot and modifying the width of the generated z vertex distribution. The latter two effects each contribute a 1% shift in the acceptance.

In a similar fashion, using the different generator tunes results in a 2% shift in the reconstruction efficiency. An additional series of checks was performed by varying the cuts imposed during the track selection and in the determination of the corresponding MC-based corrections. The resulting variation in the corrected results contributes another 1% to the reconstruction efficiency uncertainty.

Since the dependence of the reconstruction efficiency on local hit density has been parametrised in terms of leading-jet transverse energy, both the uncertainty on the jet energy scale and the accuracy of the jet-fragmentation description become relevant. The former contribution is estimated by convolving the dependence of the tracking efficiency on the leading-jet transverse energy (see Fig. 2b) with a 4% uncertainty in the jet energy scale [33]. The latter contribution is estimated by comparing the PYTHIA-based corrections to HERWIG++ [37]. The resulting p_{T}-dependent uncertainty on the occupancy is in the range (0.0–2.8)%.

Based on studies of different generator tunes and MC samples with different hard-scattering scales, the assigned uncertainty to the misidentified-track correction grows linearly as a function of p_{T} from 0.3 to 3.0%. An additional check was performed for tracks with p_{T} above 10 GeV/c to correlate the reconstructed track momentum with the deposited energy in the projected ECAL and HCAL cells. For the selected tracks in this analysis, there is no evidence of any excess of high-p_{T} misidentified tracks characterised by atypically little energy deposited in the calorimeters. The correction for secondaries and feed-down from weak decays is assigned a 1% systematic uncertainty, which is large compared to the scale of the contributions, but intended to account for the uncertainties in the $\mathrm{K}^0_{\mathrm{S}}$ and Λ fractions [38].

The tendency for finite bin widths (up to 40 GeV/c) and a finite transverse momentum resolution (rising from 1 to 5% in the range p_{T} = 10–150 GeV/c) to deform a steeply falling spectrum is corrected based on the shape of the p_{T} spectrum and the MC-based p_{T} response matrix. The effect of momentum resolution alone is 0.5–2.5%, while the wide binning results in an additional correction ranging from a fraction of a percent up to approximately 20% in the widest high-p_{T} bins. The correction for the two effects is determined by fitting an empirical function to the differential yield, smearing it with the MC-based momentum resolution, re-binning into the bins of the final invariant yield, and dividing by the original fitted form. The quoted systematic uncertainty of 0.3–2.7% is estimated by varying the fitted form of the spectrum and by performing multiple iterations of the unsmearing with successively more accurate input spectra.

In addition to the uncertainties from the event selection efficiency weighting and the tracking corrections described above, the total systematic uncertainty contains a contribution from the uncertainty on the estimation of the event pileup fraction of 0.2 and 1.2% for the 0.9 and 7 TeV data, respectively. In the cases where the total integrated luminosity is used to normalise the results, this contributes an additional 4% (11%) scale uncertainty [14, 15] for $\sqrt{s}$ = 7 (0.9) TeV. Assuming that the various p_{T}-dependent contributions are uncorrelated, the total systematic uncertainty is determined from their sum in quadrature, as indicated in Table 2.

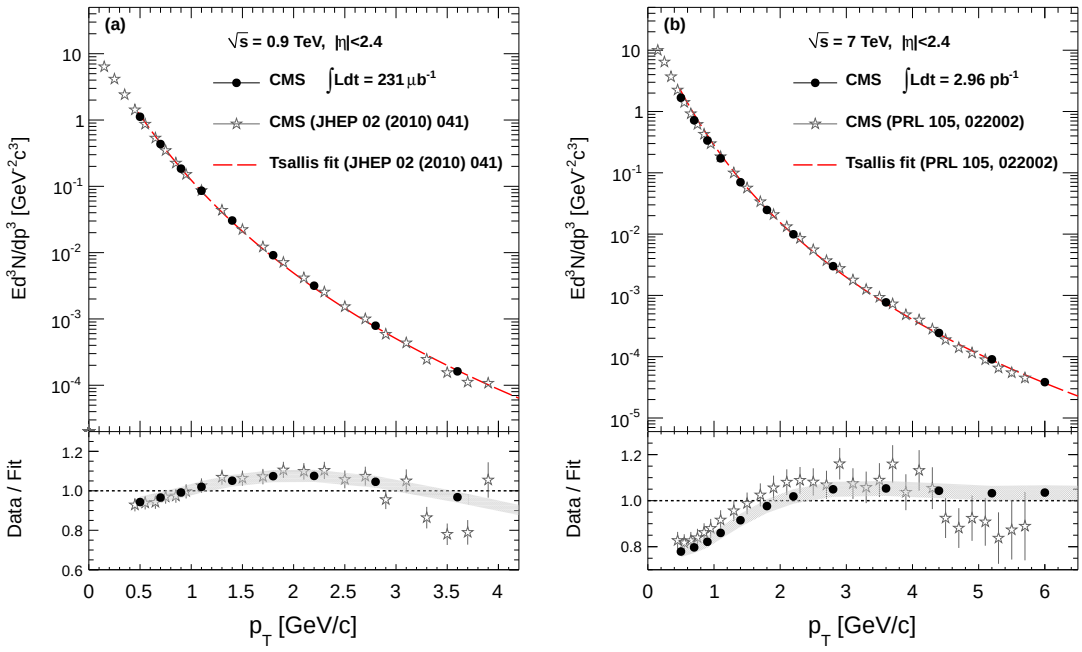

Figure 4: (a) Upper panel: the invariant charged particle differential yield from the present analysis (solid circles) and the previous CMS measurements at $\sqrt{s} = 0.9$ TeV (stars) over the limited p_T range of the earlier result. Lower panel: the ratio of the new (solid circles) and previous (stars) CMS results to a Tsallis fit of the earlier measurement. Error bars on the earlier measurement are the statistical plus systematic uncertainties added in quadrature. The systematic uncertainty band around the new measurement consists of all contributions, except for the common event selection uncertainty. (b) The same for $\sqrt{s} = 7$ TeV.

8 Results

After applying the corrections described in the previous section, the resulting invariant differential yields for charged particles within $|\eta| < 2.4$ are shown for a limited p_T range in Figs. 4a and 4b in order to quantify the agreement with previous CMS measurements at $\sqrt{s} = 0.9$ and 7 TeV [24, 34]. At each energy, both CMS measurements are divided by a Tsallis fit [39] to the earlier measurement and the ratios compared in the lower panels. For the earlier measurements, the error bars indicate the statistical plus systematic uncertainties added in quadrature. The bands around the new measurements represent all contributions to the systematic uncertainty, except the contribution from the common event selection. Statistical uncertainties are negligible on the new measurements in this p_T range. Below $p_T = 4$ GeV/c for the 0.9 TeV sample and below $p_T = 6$ GeV/c at $\sqrt{s} = 7$ TeV, which are the limits of the previously published CMS spectra, the new results are in reasonable agreement with the earlier measurements. However, the measured spectra do deviate from the Tsallis fits in the earlier papers by as much as 20% at low p_T. The origin of the small difference between the two CMS measurements at $\sqrt{s} = 7$ TeV is attributed to the different tracking algorithms used in the two measurements, as well as the different PYTHIA tunes used to determine the tracking corrections.

In the upper plots of Figs. 5a and 5b, the charged particle differential transverse momentum yields from this analysis are displayed for $\sqrt{s} = 0.9$ and 7 TeV, respectively. The latter distribution covers the p_T range up to 200 GeV/c, the largest range ever measured in a colliding beam

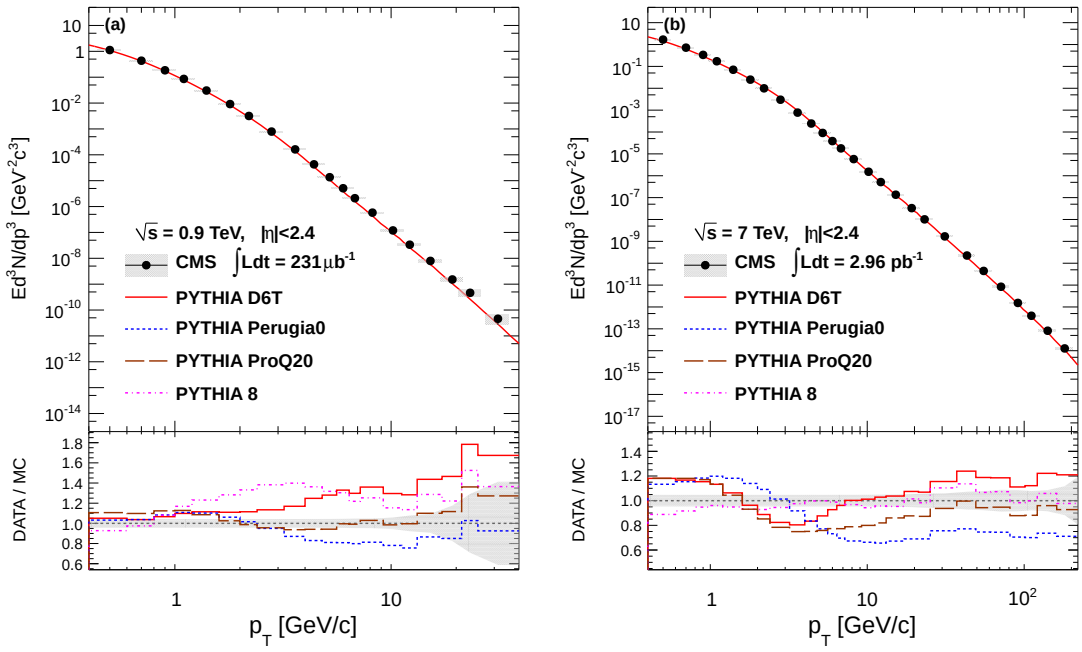

Figure 5: (a) Upper panel: the invariant charged particle differential yield at $\sqrt{s} = 0.9$ TeV compared with the predictions of four tunes of the PYTHIA MC generator. Lower panel: the ratio of the new CMS measurement to the four PYTHIA tunes. The grey band corresponds to the statistical and systematic uncertainties added in quadrature. (b) The same for $\sqrt{s} = 7$ TeV.

experiment. Also shown in the figures are various generator-level MC predictions for the yields [27, 35, 36, 40]. The lower plots of Figs. 5a and 5b show the ratios of the data to the various MC predictions. As already observed in Ref. [34], there is a deficit of $p_{\mathrm{T}} < 1$ GeV/c particles in the predicted 7 TeV spectra for several of the popular PYTHIA tunes. For the whole p_{T} range above 1 GeV/c, PYTHIA8 is the most consistent with the new 7 TeV result (within 10%). This provides an important constraint on the different generator parameters responsible for sizable variations among the tunes. A similar but slightly larger spread is observed in Fig. 5a for different generator parameters at $\sqrt{s} = 0.9$ TeV, where the CMS measurement is most consistently described by the ProQ20 tune.

As discussed in Ref. [41, 42], a robust prediction of pQCD hard processes is the power-law scaling of the inclusive charged particle invariant differential cross section with the variable x_{T}:

$$E\frac{d^3\sigma}{dp^3} = F(x_{\mathrm{T}})/p_{\mathrm{T}}^{n(x_{\mathrm{T}},\sqrt{s})} = F'(x_{\mathrm{T}})/\sqrt{s}^{n(x_{\mathrm{T}},\sqrt{s})}, \tag{4}$$

where F and F' are independent of $\sqrt{s}$, and the slow evolution of the power-law exponent n with x_{T} and $\sqrt{s}$ ($n \simeq 5$–6) is due to the running of α_{s} and changes in the parton distribution and fragmentation functions. In the upper plot of Fig. 6a, the 0.9 and 7 TeV pp measurements from this analysis are compared to the empirical scaling observed from measurements over a range of lower $\mathrm{p\bar{p}}$ collision energies by plotting $\sqrt{s}^n\, E\, d^3\sigma/dp^3$. For the purpose of reporting the CMS results as differential cross sections, the integrated luminosities for the analysed data samples were measured according to the descriptions in Ref. [14, 15]. Also, to compare with the published results from the CDF experiment at $\sqrt{s} = 0.63$, 1.8, and 1.96 TeV, the pseudorapidity

range has been restricted to $|\eta| < 1.0$. Whereas an exponent $n = 5.5$ was found in Ref. [42] from a global fit to only the previous $p\bar{p}$ measurements from $\sqrt{s} = 0.2$ to 1.96 TeV, the x_T scaling presented in this paper is optimised for use in an interpolation between the CDF and CMS measurements from $\sqrt{s} = 0.9$ to 7 TeV. Within this range, the best scaling is achieved with an exponent of $n = 4.9 \pm 0.1$. This is consistent with the predictions of next-to-leading-order (NLO) calculations, where the scaling is also found to be optimised for this value of the exponent [42]. From the lower panel of Fig. 6a, it is apparent that the NLO calculations over-predict the measured cross sections by almost a factor of two at all collision energies. This is in spite of the relatively good agreement in the inclusive jet spectrum [43, 44], which suggests that the fragmentation functions are not well tuned for LHC energies.

The CMS results are consistent over the accessible x_T range with the empirical x_T scaling given by Eq. (4) and established at lower energies. This quality of the scaling is more easily seen in the upper panel of Fig. 6b, where the points show the ratio of the various differential cross sections, scaled by $\sqrt{s}^{4.9}$, to the result of a global power-law fit to the CDF and CMS data from Fig. 6a. The fitting function is of the form $F'(x_T) = p_0 \cdot [1 + (x_T/p_1)]^{p_2}$, where p_0, p_1, and p_2 are free parameters, and the region below $p_T = 3.5\,\mathrm{GeV}/c$ has been excluded to avoid complications from soft-particle production. Considering the somewhat naïve power-law function and the expected non-scaling effects [45], the new measurement is in reasonable agreement with the global power-law fit result (within roughly 50%) over its full x_T range.

9 Interpolation to 2.76 TeV

In order to construct a predicted reference charged particle differential cross section at $\sqrt{s}$ = 2.76 TeV for comparison with the measured PbPb heavy-ion spectrum, two different techniques are used in partially overlapping transverse momentum regimes. In the high-p_T range from 5.0–200 GeV/c, where approximate x_T scaling is expected to hold, the estimated 2.76 TeV cross section is derived from a common x_T-scaling curve, based on the CDF and CMS measurements shown in Fig. 6a. In the low-p_T range from 1.0–20 GeV/c, it is possible to interpolate directly between the several measured cross section values as a function of $\sqrt{s}$ at each fixed p_T value.

As discussed in the previous section, the upper panel of Fig. 6b shows the residual difference from perfect x_T scaling with exponent $n = 4.9$ for the 0.9 and 7 TeV CMS measurements and for the 1.96 TeV CDF measurement [4, 5] . The $\sqrt{s}$ and x_T dependence of the residuals are not unexpected, since this behaviour is predicted by NLO calculations. This can be seen in the lower panel of Fig. 6b, which shows the predicted deviation from perfect x_T scaling for calculated NLO cross sections at several collision energies with respect to a reference centre-of-mass energy of 2.75 TeV [42]. The calculations were performed using the CTEQ66 parton distribution functions [46], DSS fragmentation [47], and a factorisation scale $\mu = p_T$ [42]. Taking the magnitude of the x_T-scaling violation from NLO (ranging from 0–20%), each of the three measurements in data (i.e., 0.9, 1.96, and 7 TeV) can be corrected separately to arrive at an expectation for the 2.76 TeV cross section. The three independent interpolations based on NLO-corrected x_T scaling are shown as solid blue lines in the upper panel of Fig. 6b. The combined 'best estimate' (shown as a shaded band) has an associated uncertainty that covers the deviations of up to 12% observed by varying the factorisation scale from $\mu = 0.5\,p_T$ to $\mu = 2.0\,p_T$ for each of the three collision energies. The error band is expanded below $p_T \approx 8\,\mathrm{GeV}/c$ to include the full difference between the 1.96 and 7 TeV results, since the evolution of the spectra below this value — corresponding to $x_T = 0.0023$ (7 TeV), 0.0082 (1.96 TeV), and 0.018 (0.9 TeV) — is no longer consistently described by x_T scaling and the NLO-based corrections. In addition to the 12% contribution from the uncertainty on the NLO-based correction, the final uncertainty on

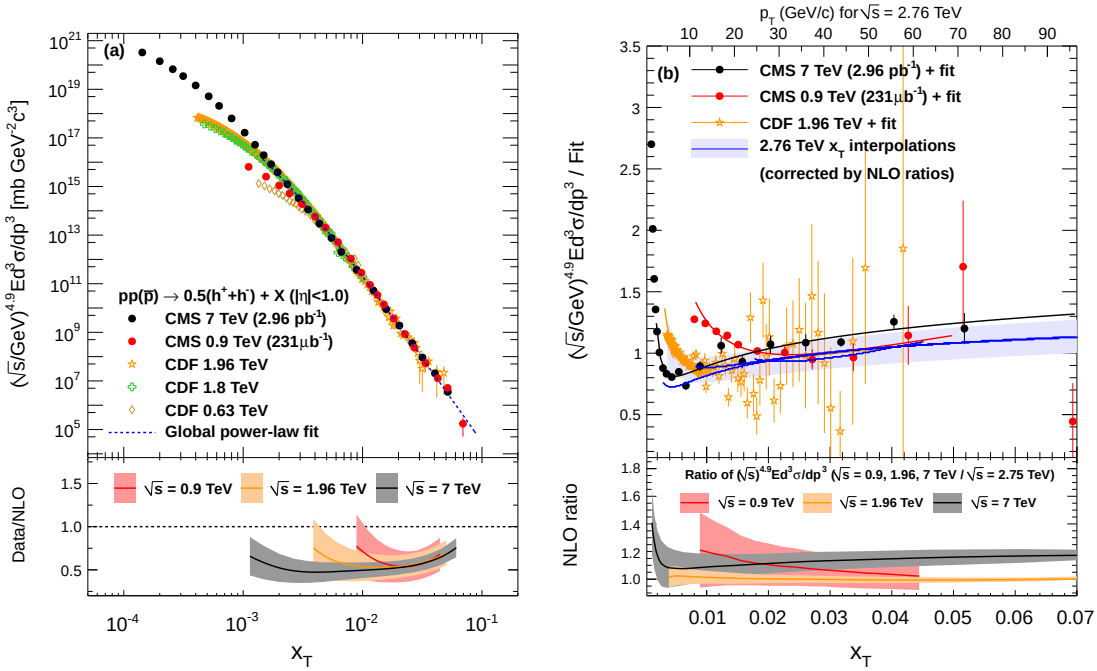

Figure 6: (a) Upper panel: inclusive charged particle invariant differential cross sections, scaled by $\sqrt{s}^{4.9}$, for $|\eta| < 1.0$ as a function of the scaling parameter x_{T}. The result is the average of the positive and negative charged particles. Lower panel: ratios of differential cross sections measured at 0.9, 1.96, and 7 TeV to those predicted by NLO calculations for factorisation scales ranging from 0.5–2.0 p_{T}. (b) Upper panel: ratios of the scaled differential cross sections to the global power-law x_{T} fit described in the text (coloured markers) and fits to these ratios (similarly coloured thin lines). The expected ratio for $\sqrt{s} = 2.76$ TeV after applying NLO-based corrections to each of the three measurements as described in the text (solid blue lines). The uncertainty from the NLO parameters is represented by the shaded band. The upper axis translates x_{T} to p_{T} for $\sqrt{s} = 2.76$ TeV. Lower panel: ratios of the NLO-calculated cross sections at three different energies, scaled by $\sqrt{s}^{4.9}$, to the cross section calculated at $\sqrt{s} = 2.75$ TeV. The width of the bands represents the variation of the factorisation scale by a factor of two.

the interpolated cross section has an additional component to account for possible correlations in the luminosity uncertainty between the three measurements. This term, taken as equal to the smallest individual uncertainty (4%), is added in quadrature.

The direct interpolation of cross sections at a fixed value of p_{T} is done using CDF measurements at $\sqrt{s} = 0.63, 1.8$ and 1.96 TeV [4, 5, 17], the new CMS measurements at $\sqrt{s} = 0.9$ and 7 TeV, as well as an earlier result at $\sqrt{s} = 2.36$ TeV [24]. The latter measurement is converted to a differential cross section assuming the total inelastic cross section of 60.52 mb from PYTHIA. At each energy, an empirical fit to the p_{T} distribution is first constructed to provide a continuous estimation independent of different binning. Then, in arbitrarily small p_{T} bins, these empirical fits are evaluated and the evolution of the cross section with $\sqrt{s}$ is parametrised by a second-order polynomial. Two examples of these fits are shown in Fig. 7a for $p_{\mathrm{T}} = 3$ and 9 GeV/c. The uncertainty on the value of the fit evaluated at $\sqrt{s} = 2.76$ TeV is taken from the covariance matrix of the fit terms, with an additional 4% added in quadrature to account conservatively for any correlation in the luminosity uncertainty between the different measurements.

To arrive at a single interpolated spectrum over the full p_T range, a linear combination of the two techniques is used with weights that vary linearly across the overlap range from $p_T = 5\,\text{GeV}/c$ (only direct interpolation at fixed p_T) to $p_T = 20\,\text{GeV}/c$ (only x_T scaling with NLO-based residual correction). In the p_T range where the two techniques overlap, the different methods agree to within their respective systematic uncertainties. (The fixed-p_T interpolation value is typically around 8% lower than the x_T interpolation.) The resulting predicted 2.76 TeV differential cross section is shown in the upper panel of Fig. 7b, and its ratio with respect to various PYTHIA tunes at that centre-of-mass energy in the lower panel. The uncertainty on the predicted cross section, shown by the grey band in the lower panel, is the weighted sum (where applicable) of the uncertainties derived from the two methods described in the preceding paragraphs. Also shown in the lower panel of Fig. 7b is the ratio of the predicted 2.76 TeV cross section to that found by simply scaling the CMS measured 7 TeV result by the expected 2.75 TeV to 7 TeV ratio from NLO calculations [42]. The interpolation used in the recent ALICE publication [13] is a few percent lower than the result quoted in this paper, but consistent within the respective systematic uncertainties. The behavior of the various generators compared to the interpolated 2.76 TeV cross section is broadly similar to the 0.9 TeV invariant yields presented in Fig. 7b. The ProQ20 tune agrees most closely (within 15%) with the interpolated cross section above 2 GeV/c. Future analysis of a recently recorded 2.76 TeV pp collision sample will provide verification of this result and a reduction in the systematic uncertainties.

10 Summary

In this paper, measurements of the phase-space-invariant differential yield $E\,d^3N_{\text{ch}}/dp^3$ at $\sqrt{s}$ = 0.9 and 7 TeV have been presented for primary charged particles, averaged over the pseudorapidity acceptance of the CMS tracking system ($|\eta| < 2.4$). The results have been shown to be in reasonable agreement with the previously published CMS measurements at $\sqrt{s}$ = 0.9 and 7 TeV [24, 34] and, except for the surplus of tracks at very low transverse momentum, with PYTHIA leading-order pQCD. The 7 TeV data are most consistent with PYTHIA8, which agrees at the 10% level over the full p_T range of the measurement. In contrast, the 0.9 TeV data are considerably better described by the ProQ20 tune. Additionally, the consistency of the 0.9 and 7 TeV spectra has been demonstrated with an empirical x_T scaling that unifies the differential cross sections from a wide range of collision energies onto a common curve. Furthermore, within the theoretical uncertainties of the NLO calculations, the residual breaking of x_T scaling above $p_T \approx 8\,\text{GeV}/c$ is consistent between the measured cross sections and the NLO calculations.

This result has removed a large uncertainty from an important ingredient of existing and future PbPb measurements, namely the pp reference spectrum corresponding to the energy of the 2010 PbPb run: 2.76 TeV per nucleon. By employing a combination of techniques to interpolate between the results presented here at $\sqrt{s} = 0.9$ and 7 TeV, including information from existing CDF measurements at $\sqrt{s} = 0.63$, 1.8, and 1.96 TeV, a pp reference at $\sqrt{s} = 2.76$ TeV has been constructed over a large range of transverse momentum (p_T = 1–100 GeV/c) with systematic uncertainties of less than 13%.

Acknowledgements

We wish to congratulate our colleagues in the CERN accelerator departments for the excellent performance of the LHC machine. We thank the technical and administrative staff at CERN and other CMS institutes, and acknowledge support from: FMSR (Austria); FNRS and FWO (Belgium); CNPq, CAPES, FAPERJ, and FAPESP (Brazil); MES (Bulgaria); CERN; CAS, MoST, and

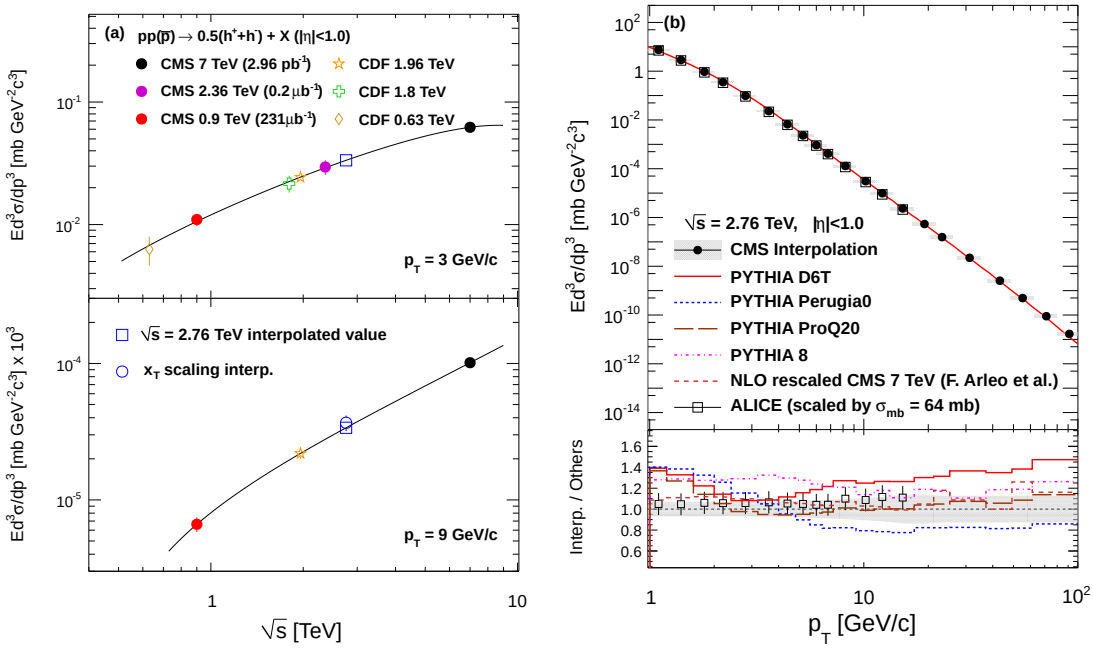

Figure 7: (a) Interpolations between measured charged particle differential cross sections at different $\sqrt{s}$ for the two example values of $p_{\mathrm{T}} = 3$ and $9\,\mathrm{GeV}/c$. Second-order polynomial fits to the measured data are shown by the solid lines. The open squares show the resulting interpolated cross sections for $\sqrt{s} = 2.76\,\mathrm{TeV}$. The open circle on the lower panel represents the corresponding estimate from the x_{T}-scaling approach in the overlap region where both can be estimated. (b) Upper panel: the predicted 2.76 TeV charged particle differential transverse momentum cross section, based on the combined direct p_{T} interpolation and NLO-corrected x_{T}-scaling techniques described in the text. Lower panel: ratios of combined interpolation to predictions from several PYTHIA tunes, an NLO-based rescaling approach [42], and the ALICE interpolation used in Ref. [13].

NSFC (China); COLCIENCIAS (Colombia); MSES (Croatia); RPF (Cyprus); Academy of Sciences and NICPB (Estonia); Academy of Finland, MEC, and HIP (Finland); CEA and CNRS/IN2P3 (France); BMBF, DFG, and HGF (Germany); GSRT (Greece); OTKA and NKTH (Hungary); DAE and DST (India); IPM (Iran); SFI (Ireland); INFN (Italy); NRF and WCU (Korea); LAS (Lithuania); CINVESTAV, CONACYT, SEP, and UASLP-FAI (Mexico); PAEC (Pakistan); SCSR (Poland); FCT (Portugal); JINR (Armenia, Belarus, Georgia, Ukraine, Uzbekistan); MST and MAE (Russia); MSTD (Serbia); MICINN and CPAN (Spain); Swiss Funding Agencies (Switzerland); NSC (Taipei); TUBITAK and TAEK (Turkey); STFC (United Kingdom); DOE and NSF (USA). Individuals have received support from the Marie-Curie programme and the European Research Council (European Union); the Leventis Foundation; the A. P. Sloan Foundation; the Alexander von Humboldt Foundation; the Associazione per lo Sviluppo Scientifico e Tecnologico del Piemonte (Italy); the Belgian Federal Science Policy Office; the Fonds pour la Formation à la Recherche dans l'Industrie et dans l'Agriculture (FRIA-Belgium); and the Agentschap voor Innovatie door Wetenschap en Technologie (IWT-Belgium).

References

[1] F. Arleo and D. d'Enterria, "Single inclusive pion p_T-spectra in proton-proton collisions at $\sqrt{s}$ = 22.4 GeV: data versus perturbative QCD calculations", *Phys. Rev.* **D78** (2008) 094004, arXiv:0807.1252. doi:10.1103/PhysRevD.78.094004.

[2] PHENIX Collaboration, "Inclusive cross section and double helicity asymmetry for π^0 production in $p+p$ collisions at $\sqrt{s}$ = 200 GeV: Implications for the polarized gluon distribution in the proton", *Phys. Rev.* **D76** (2007) 051106, arXiv:0704.3599. doi:10.1103/PhysRevD.76.051106.

[3] PHENIX Collaboration, "Inclusive cross section and double helicity asymmetry for π^0 production in $p+p$ collisions at $\sqrt{s}$ = 62.4 GeV", *Phys. Rev.* **D79** (2009) 012003, arXiv:0810.0701. doi:10.1103/PhysRevD.79.012003.

[4] CDF Collaboration, "Measurement of Particle Production and Inclusive Differential Cross Sections in $p\bar{p}$ Collisions at $\sqrt{s} = 1.96$ TeV", *Phys. Rev.* **D79** (2009) 112005, arXiv:0904.1098. doi:10.1103/PhysRevD.79.112005.

[5] CDF Collaboration, "Erratum: Measurement of particle production and inclusive differential cross sections in $p\bar{p}$ collisions at $\sqrt{s} = 1.96$ *TeV* [*Phys. Rev.* **D79** (2009) 112005]", *Phys. Rev.* **D82** (2010) 119903, arXiv:0904.1098. doi:10.1103/PhysRevD.82.119903.

[6] ATLAS Collaboration, "Charged-particle multiplicities in pp interactions measured with the ATLAS detector at the LHC", arXiv:1012.5104.

[7] ALICE Collaboration, "Transverse momentum spectra of charged particles in proton-proton collisions at $\sqrt{s} = 900$ GeV with ALICE at the LHC", *Phys. Lett.* **B693** (2010) 53, arXiv:1007.0719. doi:10.1016/j.physletb.2010.08.026.

[8] A. S. Yoon, E. Wenger, and G. Roland, "Convoluting jet spectra with fragmentation functions: a cross-check of the charged particle p_T spectrum", arXiv:1003.5928.

[9] B. B. Back et al., "The PHOBOS perspective on discoveries at RHIC", *Nucl. Phys.* **A757** (2005) 28. doi:10.1016/j.nuclphysa.2005.03.084.

[10] STAR Collaboration, "Experimental and theoretical challenges in the search for the quark gluon plasma: The STAR collaboration's critical assessment of the evidence from RHIC collisions", *Nucl. Phys.* **A757** (2005) 102. doi:10.1016/j.nuclphysa.2005.03.085.

[11] PHENIX Collaboration, "Formation of dense partonic matter in relativistic nucleus nucleus collisions at RHIC: Experimental evaluation by the PHENIX collaboration", *Nucl. Phys.* **A757** (2005) 184. doi:10.1016/j.nuclphysa.2005.03.086.

[12] BRAHMS Collaboration, "Quark gluon plasma and color glass condensate at RHIC? The perspective from the BRAHMS experiment", *Nucl. Phys.* **A757** (2005) 1. doi:10.1016/j.nuclphysa.2005.02.130.

[13] ALICE Collaboration, "Suppression of Charged Particle Production at Large Transverse Momentum in Central Pb–Pb Collisions at $\sqrt{s_{NN}} = 2.76$ TeV", *Phys. Lett.* **B696** (2011) 30, arXiv:1012.1004. doi:10.1016/j.physletb.2010.12.020.

[14] CMS Collaboration, "Measurement of CMS Luminosity", *CMS Physics Analysis Summary* **CMS-PAS-EWK-10-004** (2010).

[15] CMS Collaboration, "Absolute luminosity normalization", *CMS Detector Performance Summary* **CMS-DP-2011-002** (2011).

[16] UA1 Collaboration, "A Study of the General Characteristics of Proton-Antiproton Collisions at $\sqrt{s}$ = 0.2 to 0.9 TeV", *Nucl. Phys.* **B335** (1990) 261. doi:10.1016/0550-3213(90)90493-W.

[17] CDF Collaboration, "Transverse momentum distributions of charged particles produced in $\bar{p}p$ interactions at $\sqrt{s} = 630$ GeV and 1800 GeV", *Phys. Rev. Lett.* **61** (1988) 1819. doi:10.1103/PhysRevLett.61.1819.

[18] CMS Collaboration, "The CMS experiment at the CERN LHC", *JINST* **3** (2008) S08004. doi:10.1088/1748-0221/3/08/S08004.

[19] CMS Collaboration, "CMS Physics TDR: Volume I, Detector Performance and Software", *CERN-LHCC* **2006-001** (2006).

[20] CMS Collaboration, "Alignment of the CMS Silicon Tracker during Commissioning with Cosmic Rays", *JINST* **5** (2010) T03009, arXiv:0910.2505. doi:10.1088/1748-0221/5/03/T03009.

[21] A. J. Bell, "Design and Construction of the Beam Scintillation Counter for CMS", Master's thesis, University of Canterbury, Christchurch, New Zealand, 2008.

[22] T. Aumeyr, "Beam Phase and Intensity Monitoring for the Compact Muon Solenoid Experiment", Master's thesis, Vienna University of Technology, Austria, 2008.

[23] GEANT4 Collaboration, "GEANT4: a simulation toolkit", *Nucl. Instrum. and Methods* **A506** (2003) 250. doi:10.1016/S0168-9002(03)01368-8.

[24] CMS Collaboration, "Transverse momentum and pseudorapidity distributions of charged hadrons in pp collisions at $\sqrt{s} = 0.9$ and 2.36 TeV", *JHEP* **02** (2010) 041, arXiv:1002.0621. doi:10.1007/JHEP02(2010)041.

[25] CMS Collaboration, "Tracking and Vertexing Results from First Collisions", *CMS Physics Analysis Summary* **CMS-PAS-TRK-10-001** (2010).

[26] T. Sjöstrand, S. Mrenna, and P. Z. Skands, "PYTHIA 6.4 Physics and Manual", *JHEP* **05** (2006) 026, arXiv:hep-ph/0603175.

[27] P. Bartalini and L. Fanó, eds., "Proceedings of the First Workshop on Multiple Partonic Interactions at the LHC, Perugia, Italy, October 27-31, 2008". (2009). arXiv:1003.4220.

[28] F. W. Bopp, R. Engel, and J. Ranft, "Rapidity gaps and the PHOJET Monte Carlo", arXiv:hep-ph/9803437.

[29] R. Engel, J. Ranft, and S. Roesler, "Hard diffraction in hadron-hadron interactions and in photoproduction", *Phys. Rev.* **D52** (1995) 1459, arXiv:hep-ph/9502319. doi:10.1103/PhysRevD.52.1459.

[30] F. Siklér, "Study of clustering methods to improve primary vertex finding for collider detectors", *Nucl. Instrum. Meth.* **A621** (2010) 526, arXiv:0911.2767. doi:10.1016/j.nima.2010.04.058.

[31] CMS Collaboration, "Track and vertex reconstruction in CMS", *Nucl. Instrum. Meth.* **A582** (2007) 781. doi:10.1016/j.nima.2007.07.091.

[32] M. Cacciari, G. P. Salam, and G. Soyez, "The anti-k_t jet clustering algorithm", *JHEP* **04** (2008) 063, arXiv:0802.1189. doi:10.1088/1126-6708/2008/04/063.

[33] CMS Collaboration, "Determination of the Jet Energy Scale in CMS with pp Collisions at $\sqrt{s} = 7$ TeV", *CMS Physics Analysis Summary* **CMS-PAS-JME-10-010** (2010).

[34] CMS Collaboration, "Transverse-momentum and pseudorapidity distributions of charged hadrons in pp collisions at $\sqrt{s} = 7$ TeV", *Phys. Rev. Lett.* **105** (2010) 022002, arXiv:1005.3299. doi:10.1103/PhysRevLett.105.022002.

[35] T. Sjöstrand, S. Mrenna, and P. Z. Skands, "A Brief Introduction to PYTHIA 8.1", *Comput. Phys. Commun.* **178** (2008) 852, arXiv:0710.3820. doi:10.1016/j.cpc.2008.01.036.

[36] P. Z. Skands, "The Perugia Tunes", (2009). arXiv:0905.3418.

[37] M. Bähr et al., "Herwig++ Physics and Manual", *Eur. Phys. J.* **C58** (2008) 639, arXiv:0803.0883. doi:10.1140/epjc/s10052-008-0798-9.

[38] CMS Collaboration, "Strange Particle Production in pp Collisions at $\sqrt{s} = 0.9$ and 7 TeV", (2011). arXiv:1102.4282. Submitted to *JHEP*.

[39] C. Tsallis, "Possible generalization of Boltzmann-Gibbs statistics", *Journal of Statistical Physics* **52** (1988) 479. doi:10.1007/BF01016429.

[40] A. Buckley et al., "Systematic event generator tuning for the LHC", *Eur. Phys. J.* **C65** (2010) 331, arXiv:0907.2973. doi:10.1140/epjc/s10052-009-1196-7.

[41] F. Arleo, S. J. Brodsky, D. S. Hwang et al., "Higher-Twist Dynamics in Large Transverse Momentum Hadron Production", *Phys. Rev. Lett.* **105** (2010) 062002, arXiv:0911.4604. doi:10.1103/PhysRevLett.105.062002.

[42] F. Arleo, D. d'Enterria, and A. S. Yoon, "Single-inclusive production of large-pT charged particles in hadronic collisions at TeV energies and perturbative QCD predictions", *JHEP* **06** (2010) 035, arXiv:1003.2963. doi:10.1007/JHEP06(2010)035.

[43] CMS Collaboration, "Measurement of the Inclusive Jet Cross Section in pp Collisions at sqrt(s) = 7 TeV", arXiv:1106.0208.

[44] Atlas Collaboration, "Measurement of inclusive jet and dijet cross sections in proton-proton collisions at 7 TeV centre-of-mass energy with the ATLAS detector", *Eur. Phys. J.* **C71** (2011) 1512, arXiv:1009.5908. doi:10.1140/epjc/s10052-010-1512-2.

[45] M. Stratmann, R. Sassot, and P. Zurita, "Inclusive Hadron Production in the CERN-LHC Era", arXiv:1008.0540.

[46] P. M. Nadolsky et al., "Implications of CTEQ global analysis for collider observables", *Phys. Rev.* **D78** (2008) 013004, arXiv:0802.0007. doi:10.1103/PhysRevD.78.013004.

[47] D. de Florian, R. Sassot, and M. Stratmann, "Global analysis of fragmentation functions for pions and kaons and their uncertainties", *Phys. Rev.* **D75** (2007) 114010, arXiv:hep-ph/0703242. doi:10.1103/PhysRevD.75.114010.

A The CMS Collaboration

Yerevan Physics Institute, Yerevan, Armenia
S. Chatrchyan, V. Khachatryan, A.M. Sirunyan, A. Tumasyan

Institut für Hochenergiephysik der OeAW, Wien, Austria
W. Adam, T. Bergauer, M. Dragicevic, J. Erö, C. Fabjan, M. Friedl, R. Frühwirth, V.M. Ghete, J. Hammer[1], S. Hänsel, M. Hoch, N. Hörmann, J. Hrubec, M. Jeitler, W. Kiesenhofer, M. Krammer, D. Liko, I. Mikulec, M. Pernicka, H. Rohringer, R. Schöfbeck, J. Strauss, A. Taurok, F. Teischinger, P. Wagner, W. Waltenberger, G. Walzel, E. Widl, C.-E. Wulz

National Centre for Particle and High Energy Physics, Minsk, Belarus
V. Mossolov, N. Shumeiko, J. Suarez Gonzalez

Universiteit Antwerpen, Antwerpen, Belgium
L. Benucci, E.A. De Wolf, X. Janssen, J. Maes, T. Maes, L. Mucibello, S. Ochesanu, B. Roland, R. Rougny, M. Selvaggi, H. Van Haevermaet, P. Van Mechelen, N. Van Remortel

Vrije Universiteit Brussel, Brussel, Belgium
F. Blekman, S. Blyweert, J. D'Hondt, O. Devroede, R. Gonzalez Suarez, A. Kalogeropoulos, M. Maes, W. Van Doninck, P. Van Mulders, G.P. Van Onsem, I. Villella

Université Libre de Bruxelles, Bruxelles, Belgium
O. Charaf, B. Clerbaux, G. De Lentdecker, V. Dero, A.P.R. Gay, G.H. Hammad, T. Hreus, P.E. Marage, L. Thomas, C. Vander Velde, P. Vanlaer

Ghent University, Ghent, Belgium
V. Adler, A. Cimmino, S. Costantini, M. Grunewald, B. Klein, J. Lellouch, A. Marinov, J. Mccartin, D. Ryckbosch, F. Thyssen, M. Tytgat, L. Vanelderen, P. Verwilligen, S. Walsh, N. Zaganidis

Université Catholique de Louvain, Louvain-la-Neuve, Belgium
S. Basegmez, G. Bruno, J. Caudron, L. Ceard, E. Cortina Gil, J. De Favereau De Jeneret, C. Delaere[1], D. Favart, A. Giammanco, G. Grégoire, J. Hollar, V. Lemaitre, J. Liao, O. Militaru, S. Ovyn, D. Pagano, A. Pin, K. Piotrzkowski, N. Schul

Université de Mons, Mons, Belgium
N. Beliy, T. Caebergs, E. Daubie

Centro Brasileiro de Pesquisas Fisicas, Rio de Janeiro, Brazil
G.A. Alves, D. De Jesus Damiao, M.E. Pol, M.H.G. Souza

Universidade do Estado do Rio de Janeiro, Rio de Janeiro, Brazil
W. Carvalho, E.M. Da Costa, C. De Oliveira Martins, S. Fonseca De Souza, L. Mundim, H. Nogima, V. Oguri, W.L. Prado Da Silva, A. Santoro, S.M. Silva Do Amaral, A. Sznajder, F. Torres Da Silva De Araujo

Instituto de Fisica Teorica, Universidade Estadual Paulista, Sao Paulo, Brazil
F.A. Dias, T.R. Fernandez Perez Tomei, E. M. Gregores[2], C. Lagana, F. Marinho, P.G. Mercadante[2], S.F. Novaes, Sandra S. Padula

Institute for Nuclear Research and Nuclear Energy, Sofia, Bulgaria
N. Darmenov[1], L. Dimitrov, V. Genchev[1], P. Iaydjiev[1], S. Piperov, M. Rodozov, S. Stoykova, G. Sultanov, V. Tcholakov, R. Trayanov, I. Vankov

University of Sofia, Sofia, Bulgaria
A. Dimitrov, R. Hadjiiska, A. Karadzhinova, V. Kozhuharov, L. Litov, M. Mateev, B. Pavlov, P. Petkov

Institute of High Energy Physics, Beijing, China
J.G. Bian, G.M. Chen, H.S. Chen, C.H. Jiang, D. Liang, S. Liang, X. Meng, J. Tao, J. Wang, J. Wang, X. Wang, Z. Wang, H. Xiao, M. Xu, J. Zang, Z. Zhang

State Key Lab. of Nucl. Phys. and Tech., Peking University, Beijing, China
Y. Ban, S. Guo, Y. Guo, W. Li, Y. Mao, S.J. Qian, H. Teng, L. Zhang, B. Zhu, W. Zou

Universidad de Los Andes, Bogota, Colombia
A. Cabrera, B. Gomez Moreno, A.A. Ocampo Rios, A.F. Osorio Oliveros, J.C. Sanabria

Technical University of Split, Split, Croatia
N. Godinovic, D. Lelas, K. Lelas, R. Plestina[3], D. Polic, I. Puljak

University of Split, Split, Croatia
Z. Antunovic, M. Dzelalija

Institute Rudjer Boskovic, Zagreb, Croatia
V. Brigljevic, S. Duric, K. Kadija, S. Morovic

University of Cyprus, Nicosia, Cyprus
A. Attikis, M. Galanti, J. Mousa, C. Nicolaou, F. Ptochos, P.A. Razis

Charles University, Prague, Czech Republic
M. Finger, M. Finger Jr.

Academy of Scientific Research and Technology of the Arab Republic of Egypt, Egyptian Network of High Energy Physics, Cairo, Egypt
Y. Assran[4], S. Khalil[5], M.A. Mahmoud[6]

National Institute of Chemical Physics and Biophysics, Tallinn, Estonia
A. Hektor, M. Kadastik, M. Müntel, M. Raidal, L. Rebane

Department of Physics, University of Helsinki, Helsinki, Finland
V. Azzolini, P. Eerola, G. Fedi

Helsinki Institute of Physics, Helsinki, Finland
S. Czellar, J. Härkönen, A. Heikkinen, V. Karimäki, R. Kinnunen, M.J. Kortelainen, T. Lampén, K. Lassila-Perini, S. Lehti, T. Lindén, P. Luukka, T. Mäenpää, E. Tuominen, J. Tuominiemi, E. Tuovinen, D. Ungaro, L. Wendland

Lappeenranta University of Technology, Lappeenranta, Finland
K. Banzuzi, A. Korpela, T. Tuuva

Laboratoire d'Annecy-le-Vieux de Physique des Particules, IN2P3-CNRS, Annecy-le-Vieux, France
D. Sillou

DSM/IRFU, CEA/Saclay, Gif-sur-Yvette, France
M. Besancon, S. Choudhury, M. Dejardin, D. Denegri, B. Fabbro, J.L. Faure, F. Ferri, S. Ganjour, F.X. Gentit, A. Givernaud, P. Gras, G. Hamel de Monchenault, P. Jarry, E. Locci, J. Malcles, M. Marionneau, L. Millischer, J. Rander, A. Rosowsky, I. Shreyber, M. Titov, P. Verrecchia

Laboratoire Leprince-Ringuet, Ecole Polytechnique, IN2P3-CNRS, Palaiseau, France
S. Baffioni, F. Beaudette, L. Benhabib, L. Bianchini, M. Bluj[7], C. Broutin, P. Busson, C. Charlot, T. Dahms, L. Dobrzynski, S. Elgammal, R. Granier de Cassagnac, M. Haguenauer, P. Miné, C. Mironov, C. Ochando, P. Paganini, D. Sabes, R. Salerno, Y. Sirois, C. Thiebaux, B. Wyslouch[8], A. Zabi

Institut Pluridisciplinaire Hubert Curien, Université de Strasbourg, Université de Haute Alsace Mulhouse, CNRS/IN2P3, Strasbourg, France
J.-L. Agram[9], J. Andrea, D. Bloch, D. Bodin, J.-M. Brom, M. Cardaci, E.C. Chabert, C. Collard, E. Conte[9], F. Drouhin[9], C. Ferro, J.-C. Fontaine[9], D. Gelé, U. Goerlach, S. Greder, P. Juillot, M. Karim[9], A.-C. Le Bihan, Y. Mikami, P. Van Hove

Centre de Calcul de l'Institut National de Physique Nucleaire et de Physique des Particules (IN2P3), Villeurbanne, France
F. Fassi, D. Mercier

Université de Lyon, Université Claude Bernard Lyon 1, CNRS-IN2P3, Institut de Physique Nucléaire de Lyon, Villeurbanne, France
C. Baty, S. Beauceron, N. Beaupere, M. Bedjidian, O. Bondu, G. Boudoul, D. Boumediene, H. Brun, J. Chasserat, R. Chierici, D. Contardo, P. Depasse, H. El Mamouni, J. Fay, S. Gascon, B. Ille, T. Kurca, T. Le Grand, M. Lethuillier, L. Mirabito, S. Perries, V. Sordini, S. Tosi, Y. Tschudi, P. Verdier

Institute of High Energy Physics and Informatization, Tbilisi State University, Tbilisi, Georgia
D. Lomidze

RWTH Aachen University, I. Physikalisches Institut, Aachen, Germany
G. Anagnostou, M. Edelhoff, L. Feld, N. Heracleous, O. Hindrichs, R. Jussen, K. Klein, J. Merz, N. Mohr, A. Ostapchuk, A. Perieanu, F. Raupach, J. Sammet, S. Schael, D. Sprenger, H. Weber, M. Weber, B. Wittmer

RWTH Aachen University, III. Physikalisches Institut A, Aachen, Germany
M. Ata, W. Bender, E. Dietz-Laursonn, M. Erdmann, J. Frangenheim, T. Hebbeker, A. Hinzmann, K. Hoepfner, T. Klimkovich, D. Klingebiel, P. Kreuzer, D. Lanske[†], C. Magass, M. Merschmeyer, A. Meyer, P. Papacz, H. Pieta, H. Reithler, S.A. Schmitz, L. Sonnenschein, J. Steggemann, D. Teyssier

RWTH Aachen University, III. Physikalisches Institut B, Aachen, Germany
M. Bontenackels, M. Davids, M. Duda, G. Flügge, H. Geenen, M. Giffels, W. Haj Ahmad, D. Heydhausen, T. Kress, Y. Kuessel, A. Linn, A. Nowack, L. Perchalla, O. Pooth, J. Rennefeld, P. Sauerland, A. Stahl, M. Thomas, D. Tornier, M.H. Zoeller

Deutsches Elektronen-Synchrotron, Hamburg, Germany
M. Aldaya Martin, W. Behrenhoff, U. Behrens, M. Bergholz[10], A. Bethani, K. Borras, A. Cakir, A. Campbell, E. Castro, D. Dammann, G. Eckerlin, D. Eckstein, A. Flossdorf, G. Flucke, A. Geiser, J. Hauk, H. Jung[1], M. Kasemann, I. Katkov[11], P. Katsas, C. Kleinwort, H. Kluge, A. Knutsson, M. Krämer, D. Krücker, E. Kuznetsova, W. Lange, W. Lohmann[10], R. Mankel, M. Marienfeld, I.-A. Melzer-Pellmann, A.B. Meyer, J. Mnich, A. Mussgiller, J. Olzem, D. Pitzl, A. Raspereza, A. Raval, M. Rosin, R. Schmidt[10], T. Schoerner-Sadenius, N. Sen, A. Spiridonov, M. Stein, J. Tomaszewska, R. Walsh, C. Wissing

University of Hamburg, Hamburg, Germany
C. Autermann, V. Blobel, S. Bobrovskyi, J. Draeger, H. Enderle, U. Gebbert, K. Kaschube,

G. Kaussen, R. Klanner, J. Lange, B. Mura, S. Naumann-Emme, F. Nowak, N. Pietsch, C. Sander, H. Schettler, P. Schleper, M. Schröder, T. Schum, J. Schwandt, H. Stadie, G. Steinbrück, J. Thomsen

Institut für Experimentelle Kernphysik, Karlsruhe, Germany
C. Barth, J. Bauer, V. Buege, T. Chwalek, W. De Boer, A. Dierlamm, G. Dirkes, M. Feindt, J. Gruschke, C. Hackstein, F. Hartmann, M. Heinrich, H. Held, K.H. Hoffmann, S. Honc, J.R. Komaragiri, T. Kuhr, D. Martschei, S. Mueller, Th. Müller, M. Niegel, O. Oberst, A. Oehler, J. Ott, T. Peiffer, G. Quast, K. Rabbertz, F. Ratnikov, N. Ratnikova, M. Renz, C. Saout, A. Scheurer, P. Schieferdecker, F.-P. Schilling, M. Schmanau, G. Schott, H.J. Simonis, F.M. Stober, D. Troendle, J. Wagner-Kuhr, T. Weiler, M. Zeise, V. Zhukov[11], E.B. Ziebarth

Institute of Nuclear Physics "Demokritos", Aghia Paraskevi, Greece
G. Daskalakis, T. Geralis, S. Kesisoglou, A. Kyriakis, D. Loukas, I. Manolakos, A. Markou, C. Markou, C. Mavrommatis, E. Ntomari, E. Petrakou

University of Athens, Athens, Greece
L. Gouskos, T.J. Mertzimekis, A. Panagiotou, E. Stiliaris

University of Ioánnina, Ioánnina, Greece
I. Evangelou, C. Foudas, P. Kokkas, N. Manthos, I. Papadopoulos, V. Patras, F.A. Triantis

KFKI Research Institute for Particle and Nuclear Physics, Budapest, Hungary
A. Aranyi, G. Bencze, L. Boldizsar, C. Hajdu[1], P. Hidas, D. Horvath[12], A. Kapusi, K. Krajczar[13], F. Sikler[1], G.I. Veres[13], G. Vesztergombi[13]

Institute of Nuclear Research ATOMKI, Debrecen, Hungary
N. Beni, J. Molnar, J. Palinkas, Z. Szillasi, V. Veszpremi

University of Debrecen, Debrecen, Hungary
P. Raics, Z.L. Trocsanyi, B. Ujvari

Panjab University, Chandigarh, India
S. Bansal, S.B. Beri, V. Bhatnagar, N. Dhingra, R. Gupta, M. Jindal, M. Kaur, J.M. Kohli, M.Z. Mehta, N. Nishu, L.K. Saini, A. Sharma, A.P. Singh, J.B. Singh, S.P. Singh

University of Delhi, Delhi, India
S. Ahuja, S. Bhattacharya, B.C. Choudhary, B. Gomber, P. Gupta, S. Jain, S. Jain, R. Khurana, A. Kumar, K. Ranjan, R.K. Shivpuri

Bhabha Atomic Research Centre, Mumbai, India
R.K. Choudhury, D. Dutta, S. Kailas, V. Kumar, A.K. Mohanty[1], L.M. Pant, P. Shukla

Tata Institute of Fundamental Research - EHEP, Mumbai, India
T. Aziz, M. Guchait[14], A. Gurtu, M. Maity[15], D. Majumder, G. Majumder, K. Mazumdar, G.B. Mohanty, A. Saha, K. Sudhakar, N. Wickramage

Tata Institute of Fundamental Research - HECR, Mumbai, India
S. Banerjee, S. Dugad, N.K. Mondal

Institute for Research and Fundamental Sciences (IPM), Tehran, Iran
H. Arfaei, H. Bakhshiansohi[16], S.M. Etesami, A. Fahim[16], M. Hashemi, A. Jafari[16], M. Khakzad, A. Mohammadi[17], M. Mohammadi Najafabadi, S. Paktinat Mehdiabadi, B. Safarzadeh, M. Zeinali[18]

INFN Sezione di Bari [a], Università di Bari [b], Politecnico di Bari [c], Bari, Italy
M. Abbrescia[a,b], L. Barbone[a,b], C. Calabria[a,b], A. Colaleo[a], D. Creanza[a,c], N. De Filippis[a,c,1], M. De Palma[a,b], L. Fiore[a], G. Iaselli[a,c], L. Lusito[a,b], G. Maggi[a,c], M. Maggi[a], N. Manna[a,b], B. Marangelli[a,b], S. My[a,c], S. Nuzzo[a,b], N. Pacifico[a,b], G.A. Pierro[a], A. Pompili[a,b], G. Pugliese[a,c], F. Romano[a,c], G. Roselli[a,b], G. Selvaggi[a,b], L. Silvestris[a], R. Trentadue[a], S. Tupputi[a,b], G. Zito[a]

INFN Sezione di Bologna [a], Università di Bologna [b], Bologna, Italy
G. Abbiendi[a], A.C. Benvenuti[a], D. Bonacorsi[a], S. Braibant-Giacomelli[a,b], L. Brigliadori[a], P. Capiluppi[a,b], A. Castro[a,b], F.R. Cavallo[a], M. Cuffiani[a,b], G.M. Dallavalle[a], F. Fabbri[a], A. Fanfani[a,b], D. Fasanella[a], P. Giacomelli[a], M. Giunta[a], C. Grandi[a], S. Marcellini[a], G. Masetti[b], M. Meneghelli[a,b], A. Montanari[a], F.L. Navarria[a,b], F. Odorici[a], A. Perrotta[a], F. Primavera[a], A.M. Rossi[a,b], T. Rovelli[a,b], G. Siroli[a,b], R. Travaglini[a,b]

INFN Sezione di Catania [a], Università di Catania [b], Catania, Italy
S. Albergo[a,b], G. Cappello[a,b], M. Chiorboli[a,b,1], S. Costa[a,b], A. Tricomi[a,b], C. Tuve[a]

INFN Sezione di Firenze [a], Università di Firenze [b], Firenze, Italy
G. Barbagli[a], V. Ciulli[a,b], C. Civinini[a], R. D'Alessandro[a,b], E. Focardi[a,b], S. Frosali[a,b], E. Gallo[a], S. Gonzi[a,b], P. Lenzi[a,b], M. Meschini[a], S. Paoletti[a], G. Sguazzoni[a], A. Tropiano[a,1]

INFN Laboratori Nazionali di Frascati, Frascati, Italy
L. Benussi, S. Bianco, S. Colafranceschi[19], F. Fabbri, D. Piccolo

INFN Sezione di Genova, Genova, Italy
P. Fabbricatore, R. Musenich

INFN Sezione di Milano-Biccoca [a], Università di Milano-Bicocca [b], Milano, Italy
A. Benaglia[a,b], F. De Guio[a,b,1], L. Di Matteo[a,b], S. Gennai[1], A. Ghezzi[a,b], S. Malvezzi[a], A. Martelli[a,b], A. Massironi[a,b], D. Menasce[a], L. Moroni[a], M. Paganoni[a,b], D. Pedrini[a], S. Ragazzi[a,b], N. Redaelli[a], S. Sala[a], T. Tabarelli de Fatis[a,b]

INFN Sezione di Napoli [a], Università di Napoli "Federico II" [b], Napoli, Italy
S. Buontempo[a], C.A. Carrillo Montoya[a,1], N. Cavallo[a,20], A. De Cosa[a,b], F. Fabozzi[a,20], A.O.M. Iorio[a,1], L. Lista[a], M. Merola[a,b], P. Paolucci[a]

INFN Sezione di Padova [a], Università di Padova [b], Università di Trento (Trento) [c], Padova, Italy
P. Azzi[a], N. Bacchetta[a], P. Bellan[a,b], D. Bisello[a,b], A. Branca[a], R. Carlin[a,b], P. Checchia[a], M. De Mattia[a,b], T. Dorigo[a], U. Dosselli[a], F. Fanzago[a], F. Gasparini[a,b], U. Gasparini[a,b], A. Gozzelino, S. Lacaprara[a,21], I. Lazzizzera[a,c], M. Margoni[a,b], M. Mazzucato[a], A.T. Meneguzzo[a,b], M. Nespolo[a,1], L. Perrozzi[a,1], N. Pozzobon[a,b], P. Ronchese[a,b], F. Simonetto[a,b], E. Torassa[a], M. Tosi[a,b], S. Vanini[a,b], P. Zotto[a,b], G. Zumerle[a,b]

INFN Sezione di Pavia [a], Università di Pavia [b], Pavia, Italy
P. Baesso[a,b], U. Berzano[a], S.P. Ratti[a,b], C. Riccardi[a,b], P. Torre[a,b], P. Vitulo[a,b], C. Viviani[a,b]

INFN Sezione di Perugia [a], Università di Perugia [b], Perugia, Italy
M. Biasini[a,b], G.M. Bilei[a], B. Caponeri[a,b], L. Fanò[a,b], P. Lariccia[a,b], A. Lucaroni[a,b,1], G. Mantovani[a,b], M. Menichelli[a], A. Nappi[a,b], F. Romeo[a,b], A. Santocchia[a,b], S. Taroni[a,b,1], M. Valdata[a,b]

INFN Sezione di Pisa [a], Università di Pisa [b], Scuola Normale Superiore di Pisa [c], Pisa, Italy
P. Azzurri[a,c], G. Bagliesi[a], J. Bernardini[a,b], T. Boccali[a,1], G. Broccolo[a,c], R. Castaldi[a], R.T. D'Agnolo[a,c], R. Dell'Orso[a], F. Fiori[a,b], L. Foà[a,c], A. Giassi[a], A. Kraan[a], F. Ligabue[a,c],

T. Lomtadze[a], L. Martini[a,22], A. Messineo[a,b], F. Palla[a], G. Segneri[a], A.T. Serban[a], P. Spagnolo[a], R. Tenchini[a], G. Tonelli[a,b,1], A. Venturi[a,1], P.G. Verdini[a]

INFN Sezione di Roma [a], Università di Roma "La Sapienza" [b], Roma, Italy
L. Barone[a,b], F. Cavallari[a], D. Del Re[a,b], E. Di Marco[a,b], M. Diemoz[a], D. Franci[a,b], M. Grassi[a,1], E. Longo[a,b], S. Nourbakhsh[a], G. Organtini[a,b], F. Pandolfi[a,b,1], R. Paramatti[a], S. Rahatlou[a,b], C. Rovelli[1]

INFN Sezione di Torino [a], Università di Torino [b], Università del Piemonte Orientale (Novara) [c], Torino, Italy
N. Amapane[a,b], R. Arcidiacono[a,c], S. Argiro[a,b], M. Arneodo[a,c], C. Biino[a], C. Botta[a,b,1], N. Cartiglia[a], R. Castello[a,b], M. Costa[a,b], N. Demaria[a], A. Graziano[a,b,1], C. Mariotti[a], M. Marone[a,b], S. Maselli[a], E. Migliore[a,b], G. Mila[a,b], V. Monaco[a,b], M. Musich[a,b], M.M. Obertino[a,c], N. Pastrone[a], M. Pelliccioni[a,b], A. Romero[a,b], M. Ruspa[a,c], R. Sacchi[a,b], V. Sola[a,b], A. Solano[a,b], A. Staiano[a], A. Vilela Pereira[a]

INFN Sezione di Trieste [a], Università di Trieste [b], Trieste, Italy
S. Belforte[a], F. Cossutti[a], G. Della Ricca[a,b], B. Gobbo[a], D. Montanino[a,b], A. Penzo[a]

Kangwon National University, Chunchon, Korea
S.G. Heo, S.K. Nam

Kyungpook National University, Daegu, Korea
S. Chang, J. Chung, D.H. Kim, G.N. Kim, J.E. Kim, D.J. Kong, H. Park, S.R. Ro, D. Son, D.C. Son, T. Son

Chonnam National University, Institute for Universe and Elementary Particles, Kwangju, Korea
Zero Kim, J.Y. Kim, S. Song

Korea University, Seoul, Korea
S. Choi, B. Hong, M.S. Jeong, M. Jo, H. Kim, J.H. Kim, T.J. Kim, K.S. Lee, D.H. Moon, S.K. Park, H.B. Rhee, E. Seo, S. Shin, K.S. Sim

University of Seoul, Seoul, Korea
M. Choi, S. Kang, H. Kim, C. Park, I.C. Park, S. Park, G. Ryu

Sungkyunkwan University, Suwon, Korea
Y. Choi, Y.K. Choi, J. Goh, M.S. Kim, E. Kwon, J. Lee, S. Lee, H. Seo, I. Yu

Vilnius University, Vilnius, Lithuania
M.J. Bilinskas, I. Grigelionis, M. Janulis, D. Martisiute, P. Petrov, T. Sabonis

Centro de Investigacion y de Estudios Avanzados del IPN, Mexico City, Mexico
H. Castilla-Valdez, E. De La Cruz-Burelo, I. Heredia-de La Cruz, R. Lopez-Fernandez, R. Magaña Villalba, A. Sánchez-Hernández, L.M. Villasenor-Cendejas

Universidad Iberoamericana, Mexico City, Mexico
S. Carrillo Moreno, F. Vazquez Valencia

Benemerita Universidad Autonoma de Puebla, Puebla, Mexico
H.A. Salazar Ibarguen

Universidad Autónoma de San Luis Potosí, San Luis Potosí, Mexico
E. Casimiro Linares, A. Morelos Pineda, M.A. Reyes-Santos

University of Auckland, Auckland, New Zealand
D. Krofcheck, J. Tam, C.H. Yiu

University of Canterbury, Christchurch, New Zealand
P.H. Butler, R. Doesburg, H. Silverwood

National Centre for Physics, Quaid-I-Azam University, Islamabad, Pakistan
M. Ahmad, I. Ahmed, M.I. Asghar, H.R. Hoorani, W.A. Khan, T. Khurshid, S. Qazi

Institute of Experimental Physics, Faculty of Physics, University of Warsaw, Warsaw, Poland
G. Brona, M. Cwiok, W. Dominik, K. Doroba, A. Kalinowski, M. Konecki, J. Krolikowski

Soltan Institute for Nuclear Studies, Warsaw, Poland
T. Frueboes, R. Gokieli, M. Górski, M. Kazana, K. Nawrocki, K. Romanowska-Rybinska, M. Szleper, G. Wrochna, P. Zalewski

Laboratório de Instrumentação e Física Experimental de Partículas, Lisboa, Portugal
N. Almeida, P. Bargassa, A. David, P. Faccioli, P.G. Ferreira Parracho, M. Gallinaro, P. Musella, A. Nayak, P.Q. Ribeiro, J. Seixas, J. Varela

Joint Institute for Nuclear Research, Dubna, Russia
S. Afanasiev, I. Belotelov, P. Bunin, I. Golutvin, A. Kamenev, V. Karjavin, G. Kozlov, A. Lanev, P. Moisenz, V. Palichik, V. Perelygin, S. Shmatov, V. Smirnov, A. Volodko, A. Zarubin

Petersburg Nuclear Physics Institute, Gatchina (St Petersburg), Russia
V. Golovtsov, Y. Ivanov, V. Kim, P. Levchenko, V. Murzin, V. Oreshkin, I. Smirnov, V. Sulimov, L. Uvarov, S. Vavilov, A. Vorobyev, A. Vorobyev

Institute for Nuclear Research, Moscow, Russia
Yu. Andreev, A. Dermenev, S. Gninenko, N. Golubev, M. Kirsanov, N. Krasnikov, V. Matveev, A. Pashenkov, A. Toropin, S. Troitsky

Institute for Theoretical and Experimental Physics, Moscow, Russia
V. Epshteyn, V. Gavrilov, V. Kaftanov[†], M. Kossov[1], A. Krokhotin, N. Lychkovskaya, V. Popov, G. Safronov, S. Semenov, V. Stolin, E. Vlasov, A. Zhokin

Moscow State University, Moscow, Russia
E. Boos, M. Dubinin[23], L. Dudko, A. Ershov, O. Kodolova, V. Korotkikh, I. Lokhtin, A. Markina, S. Obraztsov, M. Perfilov, S. Petrushanko, L. Sarycheva, V. Savrin, A. Snigirev

P.N. Lebedev Physical Institute, Moscow, Russia
V. Andreev, M. Azarkin, I. Dremin, M. Kirakosyan, A. Leonidov, S.V. Rusakov, A. Vinogradov

State Research Center of Russian Federation, Institute for High Energy Physics, Protvino, Russia
I. Azhgirey, S. Bitioukov, V. Grishin[1], V. Kachanov, D. Konstantinov, A. Korablev, V. Krychkine, V. Petrov, R. Ryutin, S. Slabospitsky, A. Sobol, L. Tourtchanovitch, S. Troshin, N. Tyurin, A. Uzunian, A. Volkov

University of Belgrade, Faculty of Physics and Vinca Institute of Nuclear Sciences, Belgrade, Serbia
P. Adzic[24], M. Djordjevic, D. Krpic[24], J. Milosevic

Centro de Investigaciones Energéticas Medioambientales y Tecnológicas (CIEMAT), Madrid, Spain
M. Aguilar-Benitez, J. Alcaraz Maestre, P. Arce, C. Battilana, E. Calvo, M. Cepeda, M. Cerrada,

M. Chamizo Llatas, N. Colino, B. De La Cruz, A. Delgado Peris, C. Diez Pardos, D. Domínguez Vázquez, C. Fernandez Bedoya, J.P. Fernández Ramos, A. Ferrando, J. Flix, M.C. Fouz, P. Garcia-Abia, O. Gonzalez Lopez, S. Goy Lopez, J.M. Hernandez, M.I. Josa, G. Merino, J. Puerta Pelayo, I. Redondo, L. Romero, J. Santaolalla, M.S. Soares, C. Willmott

Universidad Autónoma de Madrid, Madrid, Spain
C. Albajar, G. Codispoti, J.F. de Trocóniz

Universidad de Oviedo, Oviedo, Spain
J. Cuevas, J. Fernandez Menendez, S. Folgueras, I. Gonzalez Caballero, L. Lloret Iglesias, J.M. Vizan Garcia

Instituto de Física de Cantabria (IFCA), CSIC-Universidad de Cantabria, Santander, Spain
J.A. Brochero Cifuentes, I.J. Cabrillo, A. Calderon, S.H. Chuang, J. Duarte Campderros, M. Felcini[25], M. Fernandez, G. Gomez, J. Gonzalez Sanchez, C. Jorda, P. Lobelle Pardo, A. Lopez Virto, J. Marco, R. Marco, C. Martinez Rivero, F. Matorras, F.J. Munoz Sanchez, J. Piedra Gomez[26], T. Rodrigo, A.Y. Rodríguez-Marrero, A. Ruiz-Jimeno, L. Scodellaro, M. Sobron Sanudo, I. Vila, R. Vilar Cortabitarte

CERN, European Organization for Nuclear Research, Geneva, Switzerland
D. Abbaneo, E. Auffray, G. Auzinger, P. Baillon, A.H. Ball, D. Barney, A.J. Bell[27], D. Benedetti, C. Bernet[3], W. Bialas, P. Bloch, A. Bocci, S. Bolognesi, M. Bona, H. Breuker, K. Bunkowski, T. Camporesi, G. Cerminara, J.A. Coarasa Perez, B. Curé, D. D'Enterria, A. De Roeck, S. Di Guida, N. Dupont-Sagorin, A. Elliott-Peisert, B. Frisch, W. Funk, A. Gaddi, G. Georgiou, H. Gerwig, D. Gigi, K. Gill, D. Giordano, F. Glege, R. Gomez-Reino Garrido, M. Gouzevitch, P. Govoni, S. Gowdy, L. Guiducci, M. Hansen, C. Hartl, J. Harvey, J. Hegeman, B. Hegner, H.F. Hoffmann, A. Honma, V. Innocente, P. Janot, K. Kaadze, E. Karavakis, P. Lecoq, C. Lourenço, T. Mäki, M. Malberti, L. Malgeri, M. Mannelli, L. Masetti, A. Maurisset, F. Meijers, S. Mersi, E. Meschi, R. Moser, M.U. Mozer, M. Mulders, E. Nesvold[1], M. Nguyen, T. Orimoto, L. Orsini, E. Perez, A. Petrilli, A. Pfeiffer, M. Pierini, M. Pimiä, D. Piparo, G. Polese, A. Racz, J. Rodrigues Antunes, G. Rolandi[28], T. Rommerskirchen, M. Rovere, H. Sakulin, C. Schäfer, C. Schwick, I. Segoni, A. Sharma, P. Siegrist, M. Simon, P. Sphicas[29], M. Spiropulu[23], M. Stoye, M. Tadel, P. Tropea, A. Tsirou, P. Vichoudis, M. Voutilainen, W.D. Zeuner

Paul Scherrer Institut, Villigen, Switzerland
W. Bertl, K. Deiters, W. Erdmann, K. Gabathuler, R. Horisberger, Q. Ingram, H.C. Kaestli, S. König, D. Kotlinski, U. Langenegger, F. Meier, D. Renker, T. Rohe, J. Sibille[30], A. Starodumov[31]

Institute for Particle Physics, ETH Zurich, Zurich, Switzerland
P. Bortignon, L. Caminada[32], N. Chanon, Z. Chen, S. Cittolin, G. Dissertori, M. Dittmar, J. Eugster, K. Freudenreich, C. Grab, A. Hervé, W. Hintz, P. Lecomte, W. Lustermann, C. Marchica[32], P. Martinez Ruiz del Arbol, P. Meridiani, P. Milenovic[33], F. Moortgat, C. Nägeli[32], P. Nef, F. Nessi-Tedaldi, L. Pape, F. Pauss, T. Punz, A. Rizzi, F.J. Ronga, M. Rossini, L. Sala, A.K. Sanchez, M.-C. Sawley, B. Stieger, L. Tauscher[†], A. Thea, K. Theofilatos, D. Treille, C. Urscheler, R. Wallny, M. Weber, L. Wehrli, J. Weng

Universität Zürich, Zurich, Switzerland
E. Aguiló, C. Amsler, V. Chiochia, S. De Visscher, C. Favaro, M. Ivova Rikova, B. Millan Mejias, P. Otiougova, C. Regenfus, P. Robmann, A. Schmidt, H. Snoek

National Central University, Chung-Li, Taiwan

Y.H. Chang, K.H. Chen, S. Dutta, C.M. Kuo, S.W. Li, W. Lin, Z.K. Liu, Y.J. Lu, D. Mekterovic, R. Volpe, J.H. Wu, S.S. Yu

National Taiwan University (NTU), Taipei, Taiwan
P. Bartalini, P. Chang, Y.H. Chang, Y.W. Chang, Y. Chao, K.F. Chen, W.-S. Hou, Y. Hsiung, K.Y. Kao, Y.J. Lei, R.-S. Lu, J.G. Shiu, Y.M. Tzeng, M. Wang

Cukurova University, Adana, Turkey
A. Adiguzel, M.N. Bakirci[34], S. Cerci[35], C. Dozen, I. Dumanoglu, E. Eskut, S. Girgis, G. Gokbulut, I. Hos, E.E. Kangal, A. Kayis Topaksu, G. Onengut, K. Ozdemir, S. Ozturk, A. Polatoz, K. Sogut[36], D. Sunar Cerci[35], B. Tali[35], H. Topakli[34], D. Uzun, L.N. Vergili, M. Vergili

Middle East Technical University, Physics Department, Ankara, Turkey
I.V. Akin, T. Aliev, S. Bilmis, M. Deniz, H. Gamsizkan, A.M. Guler, K. Ocalan, A. Ozpineci, M. Serin, R. Sever, U.E. Surat, E. Yildirim, M. Zeyrek

Bogazici University, Istanbul, Turkey
M. Deliomeroglu, D. Demir[37], E. Gülmez, B. Isildak, M. Kaya[38], O. Kaya[38], S. Ozkorucuklu[39], N. Sonmez[40]

National Scientific Center, Kharkov Institute of Physics and Technology, Kharkov, Ukraine
L. Levchuk

University of Bristol, Bristol, United Kingdom
F. Bostock, J.J. Brooke, T.L. Cheng, E. Clement, D. Cussans, R. Frazier, J. Goldstein, M. Grimes, M. Hansen, D. Hartley, G.P. Heath, H.F. Heath, L. Kreczko, S. Metson, D.M. Newbold[41], K. Nirunpong, A. Poll, S. Senkin, V.J. Smith, S. Ward

Rutherford Appleton Laboratory, Didcot, United Kingdom
L. Basso[42], K.W. Bell, A. Belyaev[42], C. Brew, R.M. Brown, B. Camanzi, D.J.A. Cockerill, J.A. Coughlan, K. Harder, S. Harper, J. Jackson, B.W. Kennedy, E. Olaiya, D. Petyt, B.C. Radburn-Smith, C.H. Shepherd-Themistocleous, I.R. Tomalin, W.J. Womersley, S.D. Worm

Imperial College, London, United Kingdom
R. Bainbridge, G. Ball, J. Ballin, R. Beuselinck, O. Buchmuller, D. Colling, N. Cripps, M. Cutajar, G. Davies, M. Della Negra, W. Ferguson, J. Fulcher, D. Futyan, A. Gilbert, A. Guneratne Bryer, G. Hall, Z. Hatherell, J. Hays, G. Iles, M. Jarvis, G. Karapostoli, L. Lyons, B.C. MacEvoy, A.-M. Magnan, J. Marrouche, B. Mathias, R. Nandi, J. Nash, A. Nikitenko[31], A. Papageorgiou, M. Pesaresi, K. Petridis, M. Pioppi[43], D.M. Raymond, S. Rogerson, N. Rompotis, A. Rose, M.J. Ryan, C. Seez, P. Sharp, A. Sparrow, A. Tapper, S. Tourneur, M. Vazquez Acosta, T. Virdee, S. Wakefield, N. Wardle, D. Wardrope, T. Whyntie

Brunel University, Uxbridge, United Kingdom
M. Barrett, M. Chadwick, J.E. Cole, P.R. Hobson, A. Khan, P. Kyberd, D. Leslie, W. Martin, I.D. Reid, L. Teodorescu

Baylor University, Waco, USA
K. Hatakeyama, H. Liu

Boston University, Boston, USA
T. Bose, E. Carrera Jarrin, C. Fantasia, A. Heister, J. St. John, P. Lawson, D. Lazic, J. Rohlf, D. Sperka, L. Sulak

Brown University, Providence, USA
A. Avetisyan, S. Bhattacharya, J.P. Chou, D. Cutts, A. Ferapontov, U. Heintz, S. Jabeen,

G. Kukartsev, G. Landsberg, M. Luk, M. Narain, D. Nguyen, M. Segala, T. Sinthuprasith, T. Speer, K.V. Tsang

University of California, Davis, Davis, USA
R. Breedon, M. Calderon De La Barca Sanchez, S. Chauhan, M. Chertok, J. Conway, P.T. Cox, J. Dolen, R. Erbacher, E. Friis, W. Ko, A. Kopecky, R. Lander, H. Liu, S. Maruyama, T. Miceli, M. Nikolic, D. Pellett, J. Robles, S. Salur, T. Schwarz, M. Searle, J. Smith, M. Squires, M. Tripathi, R. Vasquez Sierra, C. Veelken

University of California, Los Angeles, Los Angeles, USA
V. Andreev, K. Arisaka, D. Cline, R. Cousins, A. Deisher, J. Duris, S. Erhan, C. Farrell, J. Hauser, M. Ignatenko, C. Jarvis, C. Plager, G. Rakness, P. Schlein[†], J. Tucker, V. Valuev

University of California, Riverside, Riverside, USA
J. Babb, A. Chandra, R. Clare, J. Ellison, J.W. Gary, F. Giordano, G. Hanson, G.Y. Jeng, S.C. Kao, F. Liu, H. Liu, O.R. Long, A. Luthra, H. Nguyen, B.C. Shen[†], R. Stringer, J. Sturdy, S. Sumowidagdo, R. Wilken, S. Wimpenny

University of California, San Diego, La Jolla, USA
W. Andrews, J.G. Branson, G.B. Cerati, E. Dusinberre, D. Evans, F. Golf, A. Holzner, R. Kelley, M. Lebourgeois, J. Letts, B. Mangano, S. Padhi, C. Palmer, G. Petrucciani, H. Pi, M. Pieri, R. Ranieri, M. Sani, V. Sharma, S. Simon, Y. Tu, A. Vartak, S. Wasserbaech[44], F. Würthwein, A. Yagil, J. Yoo

University of California, Santa Barbara, Santa Barbara, USA
D. Barge, R. Bellan, C. Campagnari, M. D'Alfonso, T. Danielson, K. Flowers, P. Geffert, J. Incandela, C. Justus, P. Kalavase, S.A. Koay, D. Kovalskyi, V. Krutelyov, S. Lowette, N. Mccoll, V. Pavlunin, F. Rebassoo, J. Ribnik, J. Richman, R. Rossin, D. Stuart, W. To, J.R. Vlimant

California Institute of Technology, Pasadena, USA
A. Apresyan, A. Bornheim, J. Bunn, Y. Chen, M. Gataullin, Y. Ma, A. Mott, H.B. Newman, C. Rogan, K. Shin, V. Timciuc, P. Traczyk, J. Veverka, R. Wilkinson, Y. Yang, R.Y. Zhu

Carnegie Mellon University, Pittsburgh, USA
B. Akgun, R. Carroll, T. Ferguson, Y. Iiyama, D.W. Jang, S.Y. Jun, Y.F. Liu, M. Paulini, J. Russ, H. Vogel, I. Vorobiev

University of Colorado at Boulder, Boulder, USA
J.P. Cumalat, M.E. Dinardo, B.R. Drell, C.J. Edelmaier, W.T. Ford, A. Gaz, B. Heyburn, E. Luiggi Lopez, U. Nauenberg, J.G. Smith, K. Stenson, K.A. Ulmer, S.R. Wagner, S.L. Zang

Cornell University, Ithaca, USA
L. Agostino, J. Alexander, D. Cassel, A. Chatterjee, S. Das, N. Eggert, L.K. Gibbons, B. Heltsley, W. Hopkins, A. Khukhunaishvili, B. Kreis, G. Nicolas Kaufman, J.R. Patterson, D. Puigh, A. Ryd, E. Salvati, X. Shi, W. Sun, W.D. Teo, J. Thom, J. Thompson, J. Vaughan, Y. Weng, L. Winstrom, P. Wittich

Fairfield University, Fairfield, USA
A. Biselli, G. Cirino, D. Winn

Fermi National Accelerator Laboratory, Batavia, USA
S. Abdullin, M. Albrow, J. Anderson, G. Apollinari, M. Atac, J.A. Bakken, S. Banerjee, L.A.T. Bauerdick, A. Beretvas, J. Berryhill, P.C. Bhat, I. Bloch, F. Borcherding, K. Burkett, J.N. Butler, V. Chetluru, H.W.K. Cheung, F. Chlebana, S. Cihangir, W. Cooper, D.P. Eartly, V.D. Elvira, S. Esen, I. Fisk, J. Freeman, Y. Gao, E. Gottschalk, D. Green, K. Gunthoti,

O. Gutsche, J. Hanlon, R.M. Harris, J. Hirschauer, B. Hooberman, H. Jensen, M. Johnson, U. Joshi, R. Khatiwada, B. Klima, K. Kousouris, S. Kunori, S. Kwan, C. Leonidopoulos, P. Limon, D. Lincoln, R. Lipton, J. Lykken, K. Maeshima, J.M. Marraffino, D. Mason, P. McBride, T. Miao, K. Mishra, S. Mrenna, Y. Musienko[45], C. Newman-Holmes, V. O'Dell, R. Pordes, O. Prokofyev, N. Saoulidou, E. Sexton-Kennedy, S. Sharma, W.J. Spalding, L. Spiegel, P. Tan, L. Taylor, S. Tkaczyk, L. Uplegger, E.W. Vaandering, R. Vidal, J. Whitmore, W. Wu, F. Yang, F. Yumiceva, J.C. Yun

University of Florida, Gainesville, USA
D. Acosta, P. Avery, D. Bourilkov, M. Chen, M. De Gruttola, G.P. Di Giovanni, D. Dobur, A. Drozdetskiy, R.D. Field, M. Fisher, Y. Fu, I.K. Furic, J. Gartner, B. Kim, J. Konigsberg, A. Korytov, A. Kropivnitskaya, T. Kypreos, K. Matchev, G. Mitselmakher, L. Muniz, C. Prescott, R. Remington, M. Schmitt, B. Scurlock, P. Sellers, N. Skhirtladze, M. Snowball, D. Wang, J. Yelton, M. Zakaria

Florida International University, Miami, USA
C. Ceron, V. Gaultney, L. Kramer, L.M. Lebolo, S. Linn, P. Markowitz, G. Martinez, D. Mesa, J.L. Rodriguez

Florida State University, Tallahassee, USA
T. Adams, A. Askew, J. Bochenek, J. Chen, B. Diamond, S.V. Gleyzer, J. Haas, S. Hagopian, V. Hagopian, M. Jenkins, K.F. Johnson, H. Prosper, L. Quertenmont, S. Sekmen, V. Veeraraghavan

Florida Institute of Technology, Melbourne, USA
M.M. Baarmand, B. Dorney, S. Guragain, M. Hohlmann, H. Kalakhety, R. Ralich, I. Vodopiyanov

University of Illinois at Chicago (UIC), Chicago, USA
M.R. Adams, I.M. Anghel, L. Apanasevich, Y. Bai, V.E. Bazterra, R.R. Betts, J. Callner, R. Cavanaugh, C. Dragoiu, L. Gauthier, C.E. Gerber, S. Hamdan, D.J. Hofman, S. Khalatyan, G.J. Kunde[46], F. Lacroix, M. Malek, C. O'Brien, C. Silvestre, A. Smoron, D. Strom, N. Varelas

The University of Iowa, Iowa City, USA
U. Akgun, E.A. Albayrak, B. Bilki, W. Clarida, F. Duru, C.K. Lae, E. McCliment, J.-P. Merlo, H. Mermerkaya[47], A. Mestvirishvili, A. Moeller, J. Nachtman, C.R. Newsom, E. Norbeck, J. Olson, Y. Onel, F. Ozok, S. Sen, J. Wetzel, T. Yetkin, K. Yi

Johns Hopkins University, Baltimore, USA
B.A. Barnett, B. Blumenfeld, A. Bonato, C. Eskew, D. Fehling, G. Giurgiu, A.V. Gritsan, Z.J. Guo, G. Hu, P. Maksimovic, S. Rappoccio, M. Swartz, N.V. Tran, A. Whitbeck

The University of Kansas, Lawrence, USA
P. Baringer, A. Bean, G. Benelli, O. Grachov, R.P. Kenny Iii, M. Murray, D. Noonan, S. Sanders, J.S. Wood, V. Zhukova

Kansas State University, Manhattan, USA
A.f. Barfuss, T. Bolton, I. Chakaberia, A. Ivanov, S. Khalil, M. Makouski, Y. Maravin, S. Shrestha, I. Svintradze, Z. Wan

Lawrence Livermore National Laboratory, Livermore, USA
J. Gronberg, D. Lange, D. Wright

University of Maryland, College Park, USA
A. Baden, M. Boutemeur, S.C. Eno, D. Ferencek, J.A. Gomez, N.J. Hadley, R.G. Kellogg, M. Kirn,

Y. Lu, A.C. Mignerey, K. Rossato, P. Rumerio, F. Santanastasio, A. Skuja, J. Temple, M.B. Tonjes, S.C. Tonwar, E. Twedt

Massachusetts Institute of Technology, Cambridge, USA
B. Alver, G. Bauer, J. Bendavid, W. Busza, E. Butz, I.A. Cali, M. Chan, V. Dutta, P. Everaerts, G. Gomez Ceballos, M. Goncharov, K.A. Hahn, P. Harris, Y. Kim, M. Klute, Y.-J. Lee, W. Li, C. Loizides, P.D. Luckey, T. Ma, S. Nahn, C. Paus, D. Ralph, C. Roland, G. Roland, M. Rudolph, G.S.F. Stephans, F. Stöckli, K. Sumorok, K. Sung, E.A. Wenger, S. Xie, M. Yang, Y. Yilmaz, A.S. Yoon, M. Zanetti

University of Minnesota, Minneapolis, USA
S.I. Cooper, P. Cushman, B. Dahmes, A. De Benedetti, P.R. Dudero, G. Franzoni, J. Haupt, K. Klapoetke, Y. Kubota, J. Mans, V. Rekovic, R. Rusack, M. Sasseville, A. Singovsky

University of Mississippi, University, USA
L.M. Cremaldi, R. Godang, R. Kroeger, L. Perera, R. Rahmat, D.A. Sanders, D. Summers

University of Nebraska-Lincoln, Lincoln, USA
K. Bloom, S. Bose, J. Butt, D.R. Claes, A. Dominguez, M. Eads, J. Keller, T. Kelly, I. Kravchenko, J. Lazo-Flores, H. Malbouisson, S. Malik, G.R. Snow

State University of New York at Buffalo, Buffalo, USA
U. Baur, A. Godshalk, I. Iashvili, S. Jain, A. Kharchilava, A. Kumar, S.P. Shipkowski, K. Smith

Northeastern University, Boston, USA
G. Alverson, E. Barberis, D. Baumgartel, O. Boeriu, M. Chasco, S. Reucroft, J. Swain, D. Trocino, D. Wood, J. Zhang

Northwestern University, Evanston, USA
A. Anastassov, A. Kubik, N. Odell, R.A. Ofierzynski, B. Pollack, A. Pozdnyakov, M. Schmitt, S. Stoynev, M. Velasco, S. Won

University of Notre Dame, Notre Dame, USA
L. Antonelli, D. Berry, M. Hildreth, C. Jessop, D.J. Karmgard, J. Kolb, T. Kolberg, K. Lannon, W. Luo, S. Lynch, N. Marinelli, D.M. Morse, T. Pearson, R. Ruchti, J. Slaunwhite, N. Valls, M. Wayne, J. Ziegler

The Ohio State University, Columbus, USA
B. Bylsma, L.S. Durkin, J. Gu, C. Hill, P. Killewald, K. Kotov, T.Y. Ling, M. Rodenburg, G. Williams

Princeton University, Princeton, USA
N. Adam, E. Berry, P. Elmer, D. Gerbaudo, V. Halyo, P. Hebda, A. Hunt, J. Jones, E. Laird, D. Lopes Pegna, D. Marlow, T. Medvedeva, M. Mooney, J. Olsen, P. Piroué, X. Quan, H. Saka, D. Stickland, C. Tully, J.S. Werner, A. Zuranski

University of Puerto Rico, Mayaguez, USA
J.G. Acosta, X.T. Huang, A. Lopez, H. Mendez, S. Oliveros, J.E. Ramirez Vargas, A. Zatserklyaniy

Purdue University, West Lafayette, USA
E. Alagoz, V.E. Barnes, G. Bolla, L. Borrello, D. Bortoletto, A. Everett, A.F. Garfinkel, L. Gutay, Z. Hu, M. Jones, O. Koybasi, M. Kress, A.T. Laasanen, N. Leonardo, C. Liu, V. Maroussov, P. Merkel, D.H. Miller, N. Neumeister, I. Shipsey, D. Silvers, A. Svyatkovskiy, H.D. Yoo, J. Zablocki, Y. Zheng

Purdue University Calumet, Hammond, USA
P. Jindal, N. Parashar

Rice University, Houston, USA
C. Boulahouache, V. Cuplov, K.M. Ecklund, F.J.M. Geurts, B.P. Padley, R. Redjimi, J. Roberts, J. Zabel

University of Rochester, Rochester, USA
B. Betchart, A. Bodek, Y.S. Chung, R. Covarelli, P. de Barbaro, R. Demina, Y. Eshaq, H. Flacher, A. Garcia-Bellido, P. Goldenzweig, Y. Gotra, J. Han, A. Harel, D.C. Miner, D. Orbaker, G. Petrillo, D. Vishnevskiy, M. Zielinski

The Rockefeller University, New York, USA
A. Bhatti, R. Ciesielski, L. Demortier, K. Goulianos, G. Lungu, S. Malik, C. Mesropian, M. Yan

Rutgers, the State University of New Jersey, Piscataway, USA
O. Atramentov, A. Barker, D. Duggan, Y. Gershtein, R. Gray, E. Halkiadakis, D. Hidas, D. Hits, A. Lath, S. Panwalkar, R. Patel, A. Richards, K. Rose, S. Schnetzer, S. Somalwar, R. Stone, S. Thomas

University of Tennessee, Knoxville, USA
G. Cerizza, M. Hollingsworth, S. Spanier, Z.C. Yang, A. York

Texas A&M University, College Station, USA
R. Eusebi, J. Gilmore, A. Gurrola, T. Kamon, V. Khotilovich, R. Montalvo, I. Osipenkov, Y. Pakhotin, J. Pivarski, A. Safonov, S. Sengupta, A. Tatarinov, D. Toback, M. Weinberger

Texas Tech University, Lubbock, USA
N. Akchurin, C. Bardak, J. Damgov, C. Jeong, K. Kovitanggoon, S.W. Lee, P. Mane, Y. Roh, A. Sill, I. Volobouev, R. Wigmans, E. Yazgan

Vanderbilt University, Nashville, USA
E. Appelt, E. Brownson, D. Engh, C. Florez, W. Gabella, M. Issah, W. Johns, P. Kurt, C. Maguire, A. Melo, P. Sheldon, B. Snook, S. Tuo, J. Velkovska

University of Virginia, Charlottesville, USA
M.W. Arenton, M. Balazs, S. Boutle, B. Cox, B. Francis, R. Hirosky, A. Ledovskoy, C. Lin, C. Neu, R. Yohay

Wayne State University, Detroit, USA
S. Gollapinni, R. Harr, P.E. Karchin, P. Lamichhane, M. Mattson, C. Milstène, A. Sakharov

University of Wisconsin, Madison, USA
M. Anderson, M. Bachtis, J.N. Bellinger, D. Carlsmith, S. Dasu, J. Efron, K. Flood, L. Gray, K.S. Grogg, M. Grothe, R. Hall-Wilton, M. Herndon, P. Klabbers, J. Klukas, A. Lanaro, C. Lazaridis, J. Leonard, R. Loveless, A. Mohapatra, F. Palmonari, D. Reeder, I. Ross, A. Savin, W.H. Smith, J. Swanson, M. Weinberg

†: Deceased
1: Also at CERN, European Organization for Nuclear Research, Geneva, Switzerland
2: Also at Universidade Federal do ABC, Santo Andre, Brazil
3: Also at Laboratoire Leprince-Ringuet, Ecole Polytechnique, IN2P3-CNRS, Palaiseau, France
4: Also at Suez Canal University, Suez, Egypt
5: Also at British University, Cairo, Egypt
6: Also at Fayoum University, El-Fayoum, Egypt

7: Also at Soltan Institute for Nuclear Studies, Warsaw, Poland
8: Also at Massachusetts Institute of Technology, Cambridge, USA
9: Also at Université de Haute-Alsace, Mulhouse, France
10: Also at Brandenburg University of Technology, Cottbus, Germany
11: Also at Moscow State University, Moscow, Russia
12: Also at Institute of Nuclear Research ATOMKI, Debrecen, Hungary
13: Also at Eötvös Loránd University, Budapest, Hungary
14: Also at Tata Institute of Fundamental Research - HECR, Mumbai, India
15: Also at University of Visva-Bharati, Santiniketan, India
16: Also at Sharif University of Technology, Tehran, Iran
17: Also at Shiraz University, Shiraz, Iran
18: Also at Isfahan University of Technology, Isfahan, Iran
19: Also at Facoltà Ingegneria Università di Roma "La Sapienza", Roma, Italy
20: Also at Università della Basilicata, Potenza, Italy
21: Also at Laboratori Nazionali di Legnaro dell' INFN, Legnaro, Italy
22: Also at Università degli studi di Siena, Siena, Italy
23: Also at California Institute of Technology, Pasadena, USA
24: Also at Faculty of Physics of University of Belgrade, Belgrade, Serbia
25: Also at University of California, Los Angeles, Los Angeles, USA
26: Also at University of Florida, Gainesville, USA
27: Also at Université de Genève, Geneva, Switzerland
28: Also at Scuola Normale e Sezione dell' INFN, Pisa, Italy
29: Also at University of Athens, Athens, Greece
30: Also at The University of Kansas, Lawrence, USA
31: Also at Institute for Theoretical and Experimental Physics, Moscow, Russia
32: Also at Paul Scherrer Institut, Villigen, Switzerland
33: Also at University of Belgrade, Faculty of Physics and Vinca Institute of Nuclear Sciences, Belgrade, Serbia
34: Also at Gaziosmanpasa University, Tokat, Turkey
35: Also at Adiyaman University, Adiyaman, Turkey
36: Also at Mersin University, Mersin, Turkey
37: Also at Izmir Institute of Technology, Izmir, Turkey
38: Also at Kafkas University, Kars, Turkey
39: Also at Suleyman Demirel University, Isparta, Turkey
40: Also at Ege University, Izmir, Turkey
41: Also at Rutherford Appleton Laboratory, Didcot, United Kingdom
42: Also at School of Physics and Astronomy, University of Southampton, Southampton, United Kingdom
43: Also at INFN Sezione di Perugia; Università di Perugia, Perugia, Italy
44: Also at Utah Valley University, Orem, USA
45: Also at Institute for Nuclear Research, Moscow, Russia
46: Also at Los Alamos National Laboratory, Los Alamos, USA
47: Also at Erzincan University, Erzincan, Turkey